

# Globular cluster systems in elliptical galaxies of Coma

A. Marín-Franch

*Instituto de Astrofísica de Canarias, E-38205 La Laguna, Tenerife, Spain*

amarin@ll.iac.es

and

A. Aparicio

*Instituto de Astrofísica de Canarias, E-38205 La Laguna, Tenerife, Spain*

aaaj@ll.iac.es

## ABSTRACT

Globular cluster systems of 17 elliptical galaxies have been studied in the Coma cluster of galaxies. Surface-brightness fluctuations have been used to determine total populations of globular clusters and specific frequency ( $S_N$ ) has been evaluated for each individual galaxy. Enormous differences in  $S_N$  between similar galaxies are found. In particular,  $S_N$  results vary by an order of magnitude from galaxy to galaxy. Extreme cases are the following: a) at the lower end of the range, NGC 4673 has  $S_N = 1.0 \pm 0.4$ , a surprising value for an elliptical galaxy, but typical for spiral and irregular galaxies; b) at the upper extreme, MCG +5 -31 -063 has  $S_N = 13.0 \pm 4.2$  and IC 4051  $S_N = 12.7 \pm 3.2$ , and are more likely to belong to supergiant cD galaxies than to “normal” elliptical galaxies. Furthermore, NGC 4874, the central supergiant cD galaxy of the Coma cluster, also exhibits a relatively high specific frequency ( $S_N = 9.0 \pm 2.2$ ). The other galaxies studied have  $S_N$  in the range [2, 7], the mean value being  $S_N = 5.1$ . No single scenario seems to account for the observed specific frequencies, so the history of each galaxy must be deduced individually by suitably combining the different models (*in situ*, mergers, and accretions). The possibility that Coma is formed by several subgroups is also considered. If only the galaxies of the main subgroup defined by Gurzadyan & Mazure (2001) are used, a trend in  $S_N$  arises in the sense of  $S_N$  being bigger in higher density regions. This result needs further confirmation.

*Subject headings:* galaxies:clusters:individual (Coma)–galaxies:star clusters

## 1. Introduction

Globular clusters (GCs) are thought to be among the oldest objects in the Universe; so, although they represent only a small fraction of the total luminosity of the galaxy hosting them, they provide useful information about the galaxy formation process and its initial evolutionary stages. By studying globular cluster systems (GCS), the memory of the host galaxy is probed.

A fundamental, widely used parameter describing a GCS is the specific frequency,  $S_N$ , introduced by Harris & van den Berg (1981).  $S_N$  is the number of GCs normalized to an absolute magnitude for the parent galaxy of  $M_V^{\text{TOT}} = -15$  mag:

$$S_N = N_{\text{GC}}^{\text{tot}} 10^{0.4(M_V^{\text{TOT}}+15)}, \quad (1)$$

where  $N_{\text{tot}}$  is the total number of GCs in the galaxy.  $S_N$  gives the number of GCs per unit luminosity of the host galaxy. Spiral and irregular galaxies have typical values of  $S_N \leq 1$  (van der Berg & Harris 1982). Dwarf (Durrell et al. 1996; Miller et al. 1998), elliptical (Harris & van den Berg 1981), and lenticular galaxies (Kundu & Whitmore 1998; Chapelon et al. 1999) have  $S_N$  between 2 and 6, where larger values seem to correspond to galaxies located in high-density environments (Harris 1991). Giant cDs located near the centers of rich clusters of galaxies have the largest specific frequency,  $S_N \sim 10 - 20$  (Harris & van den Berg 1981; Harris, Pritchett, & McClure 1995; Blakeslee & Tonry 1995; Bridges et al. 1996), with some exceptions (Kaisler et al. 1996).

The origin of the observed values of  $S_N$  is not clear. A basic question is whether  $S_N$  depends on the properties of the host galaxy and/or the environment. If only elliptical galaxies are considered, environmental density seems to play a fundamental role in  $S_N$  (Harris 1991). These results, which are based on the compilation of several studies of elliptical galaxies closer than the Virgo cluster, suggest that the formation of GCs has been two or three times more efficient in rich environments than in poor ones. On the other hand, the luminosity of the host galaxy also has an influence on the properties of the GCS (Harris, Harris, & McLaughlin 1998).

Forte, Martínez, & Muzzio (1982) and Muzzio (1987) have suggested that in clusters of galaxies a population of intergalactic GCs (IGCs) should exist. A galaxy could enlarge its GC population via gravitational capture of IGCs. If they are distributed according to the gravitational potential of the whole galaxy cluster, then the influence of the environment on  $S_N$  is justified (White 1987; West et al. 1995). On the other hand, Blakeslee (1997) suggested that  $S_N$  could be strongly influenced by gas removal by tidal disruption during the formation of the cluster. This idea was developed further by Blakeslee, Tonry, & Metzger

(1997). The star formation would be inhibited as a result of the gas loss, increasing  $S_N$ . Moreover, Harris et al. (1998) argued that explaining the observed  $S_N$  in M87 via gravitational capture of IGCs, requires assuming an unrealistic spatial distribution for intergalactic GCs.

The origin of the GCSs themselves in giant elliptical galaxies is still not understood. One of the main problems in understanding this phenomenon is the lack of data. The difficulty in observing distant GCSs is due to the low resolution of available telescopes and to the low brightness of the individual GCs, which are too faint to be detected even at moderate distances. At  $\sim 100$  Mpc (the distance of the Coma galaxy cluster), only the brightest GCs are visible from ground-based observations (Harris (1987) and Thompson & Valdes (1987) performed the first studies of GCSs in Coma); high-resolution telescopes (such as the *Hubble Space Telescope (HST)*, see for example Harris et al. (2000), Kavelaars et al. (2000)) and long exposure times are required to detect them directly. But the surface-brightness fluctuations (SBF) technique, which we use in this paper, allows us to detect GCSs in elliptical galaxies at distances of the order of 100 Mpc, using small to intermediate-size, ground-based telescopes and reasonable exposure times (Blakeslee & Tonry 1995).

The SBF technique was introduced by Tonry & Schneider (1988) with the aim of measuring distances. Comparing the fluctuation signals produced by the stellar population of a galaxy with SBF measurements of nearby galaxies which have externally calibrated distances, accurate estimates of distances can be obtained up to  $\sim 40$  Mpc (Tonry et al. 2000, 2001). For smaller distances, undetected GCs contribute as a perturbation of the total fluctuation signal of the galaxy. But in the case of more distant galaxies the fluctuation signal produced by the GCs, which are mostly unresolved, dominates and the contribution of stars becomes negligible (Wing et al. 1995; Blakeslee & Tonry 1995; Blakeslee, Tonry, & Metzger 1997; Blakeslee 1999).

In this paper, we use the SBF technique to evaluate the GCS properties of elliptical galaxies in the Coma cluster. Coma is a good laboratory for studying GCSs, because it is a rich cluster and its ellipticals have a wide range of luminosities and environmental densities. After describing the SBF technique and its use in obtaining GCS properties (§3), we present a test for evaluating the capacity of the technique (§4), which we then apply to the Coma cluster galaxies (§5).

## 2. Observations and Data Reduction

This study is based on observations done in 2000 April 25 and 27 with the 2.5 m INT at the Roque de los Muchachos Observatory on La Palma, using the Wide Field Camera, which consists of four  $2048 \times 4100$  pixel chips with a scale of  $0.333''/\text{pix}$ , providing a field of view per chip of  $11.38' \times 22.75'$ . The total field of view is  $\sim 34'$  on a side.

In Table 1, the location of the target fields and all the galaxies studied in each field are listed. Column 1 gives the name adopted in this article for each target field, columns 2 and 3 give the coordinates of the field and column 4 gives the galaxies analyzed in each field. Twelve exposures of 300 s with the Sloan  $R$  Filter were taken for each field, except for the central field of Coma (RC-1) where thirteen exposures of 300 s were taken; this resulted in a total integration time of 3600 s (or 3900 s for RC-1). In Table 2, a summary of the observations is given. Column 1 lists the field names, column 2 the date of the observation, columns 3 and 4 give the exposure times and the used filter, and column 5 gives the seeing, which is between  $1''$  and  $1.2''$  in all cases. The bias level was subtracted from the individual frames using the overscan region of the CCD. The data were then flattened with twilight sky flats. The final image was produced by calibrating the individual frames, dithering between exposures and calculating an average of the frames. In Fig. 1, the central chip of the CCD is shown for the target field RC-1, where nine studied galaxies are marked. This field corresponds to the center of the Coma cluster.

Photometric calibration was performed for the second night. The observations of the first night were then calibrated comparing the field RC-1 observed in both nights. The extinction and photometric calibration were calculated using five measurements of 23 Landolt (1992) standard stars. The equation transforming instrumental to standard magnitudes is

$$R - r + AX = a_i + b_i \times (V - R), \quad (2)$$

where  $R$  is the magnitude in the standard system,  $r$  is the instrumental magnitude,  $X$  is the airmass (all the observations of target objects have airmass smaller than 1.1) and  $A$  is the extinction, for which a value  $A = 0.145$  was obtained.  $(V - R)$  is the colour index of the program objects. Since no observations were done in the  $V$  Filter, a typical value for the colour index of GCs of  $(V - R) = 0.46$  was adopted (Ajhar et al. 1994).  $a_i$  and  $b_i$  are the zero point and the color term for each chip ( $i=1, 2, 3$  and  $4$ ). Our results for  $a_i$  and  $b_i$  are listed in Table 3. The sigma of the photometric calibration varies between 0.01 and 0.02 mag. Calibration results for each individual galaxy are shown in Table 4, where  $m_1^*$  is the magnitude of an object yielding one unit of flux per unit time. This magnitude will be used later. The sigma of  $m_1^*$  represents the sigma of the photometric calibration. Finally, as

Coma is nearly perpendicular to the Galactic plane, interstellar extinction is neglected.

### 3. Surface Brightness Fluctuations: the Technique

The concept of surface-brightness fluctuations was introduced by Tonry & Schneider (1988), who noted that in the surface photometry of a galaxy far enough to remain unresolved, a pixel-to-pixel fluctuation is observed due to the Poisson statistics of the spatial distribution of stars, GCs, background galaxies, foreground stars, etc. This is correct for a galaxy with no absorption or emission due to dust or gas; so this technique would only be applicable to early-type galaxies. The variance of the fluctuation depends on the stellar population, the GCS, background galaxies, foreground star, and, of course, the distance.

#### 3.1. Sources of Variance: GCS Properties

The following treatment has been described by Blakeslee & Tonry (1995). It can be assumed that the total pixel-to-pixel variance of an image ( $\sigma_{\text{TOT}}^2$ ) is the sum of all the independent contributions due to the different components in the image, such as the stellar population ( $\sigma_{\text{SP}}^2$ ), GCs ( $\sigma_{\text{GC}}^2$ ), background galaxies ( $\sigma_{\text{BG}}^2$ ), foreground stars ( $\sigma_{\text{FS}}^2$ ), read-out noise ( $\sigma_{\text{ro}}^2$ ) and photon shot noise ( $\sigma_{\text{ph}}^2$ ):

$$\sigma_{\text{TOT}}^2 = \sigma_{\text{SP}}^2 + \sigma_{\text{GC}}^2 + \sigma_{\text{BG}}^2 + \sigma_{\text{FS}}^2 + \sigma_{\text{ro}}^2 + \sigma_{\text{ph}}^2 \quad (3)$$

The pixel-to-pixel variance produced by a class of object can be evaluated as the second moment of the luminosity function of that object population. In general, the brightest individuals could be resolved in the image. For the analysis of the SBF, these objects must be masked. If all sources brighter than a limiting flux ( $f_{\text{lim}}$ ) are masked in the image, then the variance produced by the remaining part of the population is:

$$\sigma_{\text{POP}}^2 = \int_0^{f_{\text{lim}}} n(f) f^2 df, \quad (4)$$

where  $n(f)$  is the luminosity function; i.e., the number of population objects per unit flux per pixel. We can put this equation in terms of magnitudes via the relationship

$$m = -2.5 \log(f) + m_1^*, \quad (5)$$

$f$  being the flux ( $e^- \text{ s}^{-1} \text{ pix}^{-1}$ ) and  $m_1^*$  the magnitude of an object yielding one unit of flux per unit time.

If  $n(f)$  is known, the variance produced by the non-masked part of the population can be evaluated. In the case of GCs, a Gaussian shape for the luminosity function (GCLF) can be assumed (Harris 1991):

$$n_{\text{GC}}(m) = \frac{N_{\text{GC}}}{\sqrt{2\pi}\sigma} e^{-(m-m^0)^2/2\sigma^2}, \quad (6)$$

where  $N_{\text{GC}}$  is the total number of GCs per pixel. Substituting eq. 6 into eq. 4, the variance due to the non-masked globular clusters can be expressed as:

$$\sigma_{\text{GC}}^2 = \frac{N_{\text{GC}}}{\sqrt{2\pi}\sigma} 10^{0.8m_1^*} \int_{m_c}^{\infty} e^{-(m-m^0)^2/2\sigma^2} e^{-0.8\ln(10)m} dm, \quad (7)$$

where  $m_c$  is the magnitude corresponding to the limiting flux  $f_{\text{lim}}$ .

It can be seen that the variance produced by the GCs is proportional to their total surface density. In this way, assuming values for  $m^0$  and  $\sigma$  in the GCLF, and determining the variance produced by GCs,  $\sigma_{\text{GC}}^2$  from the image analysis, their surface density can be obtained. In galaxies with large angular size, the spatial structure of the GCS can be also evaluated by dividing the galaxy into rings and measuring the GCs' variance in each one.

What is directly obtained from the analysis of the image is  $\sigma_{\text{TOT}}^2$ . Hence a treatment of the remaining sources of variance is required. First, at the distance of Coma, using eq. 7 and with the help of the Padua stellar evolution library (see Bertelli et al. (1994)), it can be shown that the ratio  $\sigma_{\text{SP}}^2/\sigma_{\text{GC}}^2$  is nearly zero, so  $\sigma_{\text{SP}}^2$  can be neglected in eq. 3. Also, as Coma is nearly perpendicular to the Galactic plane, foreground stars are very few, and  $\sigma_{\text{FS}}^2$  can be neglected. Hence,

$$\sigma_{\text{TOT}}^2 \approx \sigma_{\text{GC}}^2 + \sigma_{\text{BG}}^2 + \sigma_{\text{ph}}^2 + \sigma_{\text{ro}}^2. \quad (8)$$

As we will see later, the SBF technique involves spectral analysis of the signal. This provides two quantities:  $P_1$  and  $P_0$ .  $P_0$  is the total PSF-convolved variance, produced by all objects whose spatial flux distribution is convolved with the PSF.  $P_1$  is the non-PSF-convolved variance. As a result,

$$P_0 \approx \sigma_{\text{GC}}^2 + \sigma_{\text{BG}}^2 \quad (9)$$

and

$$P_1 = \sigma_{\text{ro}}^2 + \sigma_{\text{ph}}^2. \quad (10)$$

Consequently, the only contribution to  $\sigma_{\text{TOT}}^2$  we have to be concerned with is  $\sigma_{\text{BG}}^2$ . Once this is removed,  $\sigma_{\text{GC}}^2$  will be obtained from  $P_0$ .

The following law can be assumed for the luminosity function of background galaxies (BGLF):

$$n_{\text{BG}}(m) = A \times N_{\text{BG}} 10^{\gamma m}, \quad (11)$$

where  $A$  is a constant for normalization,  $N_{\text{BG}}$  is the total number of galaxies per pixel and  $\gamma$  is the slope of the magnitude distribution. Tyson (1988) found  $\gamma \approx 0.39$  in the  $R$  filter. Using eq. 4, we find

$$\sigma_{\text{BG}}^2 = \frac{A \times N_{\text{BG}}}{\ln 10(0.8 - \gamma)} 10^{\gamma m_c} 10^{0.8(m_1^* - m_c)}. \quad (12)$$

Once the parameters  $A$ ,  $N_{\text{BG}}$  and  $m_c$  are estimated from an analysis of the image, as we will see later, and  $m_1^*$  from the photometric calibration,  $\sigma_{\text{BG}}^2$  can be calculated.

### 3.2. Measuring $\sigma_{\text{GC}}^2$

As we have seen, because stars, background galaxies, and GCs are convolved with the PSF, while the read-out and photon shot noise are not, if a power spectrum of the image is computed, the non-convolved variance can be separated from the remaining terms. The power spectrum of the image,  $P(k)$ , has the form

$$P(k) = P_1 + P_0 E(k), \quad (13)$$

where  $E(k)$  is the power spectrum of the PSF convolved with the window function (which is unity in all the regions we want to study and zero in the rest of the image),  $P_0$  is the PSF-convolved variance ( $P_0 = \sigma_{\text{SP}}^2 + \sigma_{\text{GC}}^2 + \sigma_{\text{BG}}^2 + \sigma_{\text{FS}}^2 + \dots$ ), and  $P_1$  is the non-PSF-convolved variance ( $P_1 = \sigma_{\text{ro}}^2 + \sigma_{\text{ph}}^2$ ).

Before performing the power spectrum of the image, a preliminary image treatment has to be done.

### 3.2.1. Preliminary image treatment

After the initial image reduction was done, and because there are some galaxies located in each chip of the CCD mosaic, different regions of the chips were selected, each containing a galaxy (see Fig. 1) that was treated individually. In all cases, a smooth fit of the galaxy profile was performed using the IRAF package ISOPHOTE. An iterative method was used: first, bright objects that could affect the galaxy profile fit were masked. The task ELLIPSE was used to fit this profile, and the result was subtracted from the original image in order to obtain a map of the bright objects alone. These were then subtracted from the initial image and a second fit of the galaxy profile was made. This procedure was repeated until the precision of the final fit was good enough.

Once the final galaxy profile was performed and subtracted, a residual zero mean image is obtained where the PSF-convolved variance can be measured. In this image the power spectrum is only perturbed at low wave numbers (Jensen, Tonry, & Luppino 1999), so this part of the power spectrum will not be taken into account in our analysis.

Using the DAOPHOT task DAOFIND, all the objects  $4\sigma$  above the zero mean of the residual image are selected. Those brighter than some limiting magnitude ( $m_c$ ) were masked out creating a window function whose value is zero where the bright object is located and unity in the rest of the image. The magnitude  $m_c$  must be chosen appropriately. Note that if a very bright  $m_c$  is used,  $P_0$  is dominated by the non-masked brightest objects (since it is the second moment of the luminosity function of the population which is at work). In our study, brightest objects are background galaxies, so the GC contribution is masked out. Because the CG contribution will be evaluated, as many bright objects as possible must be masked out. On the other hand, if  $m_c$  is chosen too faint, the results could be affected by incompleteness, resulting in an incorrect estimate of the unresolved background galaxy contribution to  $P_0$ . An analysis of this question has to be made in each case. In this article, we choose  $m_c = 23.5$ .

In large-angular-size galaxies, the spatial distribution of the GCS can be analyzed. In those cases, the set of ring-shaped regions in which the  $P_0$  will be measured can be defined making use of the galaxy profile fit. We can select different isophotes to define the annular sections, in this way, elliptical annular regions are obtained at different distances from the center of the galaxy. Multiplying the previous window function with each defined annular region, a set of new window functions is obtained, one for each ring that we shall be studying.



### 3.2.2. Measuring $\sigma_{\text{GC}}^2$

Multiplying the window function of a selected region by the residual image, the residual masked image of the region is obtained. After this, the power spectrum of the residual masked image is computed. The result is a two-dimensional power spectrum, which is radially averaged in order to obtain the one-dimensional power spectrum of the selected region. This has the form expressed in equation 13. In order to evaluate  $P_0$ , the power spectrum of the PSF convolved with the window function of the region is needed. But  $E(k)$  can be approximated by the power spectrum of the PSF alone,  $P_{\text{PSF}}(k)$ , with a negligible error (Jensen et al. 1998), so eq. 13 transforms into

$$P(k) = P_1 + P_0 P_{\text{PSF}}(k). \quad (14)$$

Using an empirical form for the PSF, obtained from some bright, isolated stars in the same image being analyzed, and fitting the power spectrum of the images with eq. 14, the quantities  $P_0$  and  $P_1$  can be evaluated. In large-angular-size galaxies, the spatial structure of the GCS can be deduced from the radial dependence of  $P_0$ . In the case of smaller galaxies, where we cannot measure radial dependences, only the total number of GCs is evaluated.

## 4. Testing the Technique Using Synthetic Images

Putting into practice what we have presented in the preceding sections, in this section we will make a consistency test to check our procedure for measuring the power spectrum normalization. The influence of the noise level in the images is also tested. Synthetic images were constructed with this purpose in the following manner. The magnitudes of the GC were randomly calculated according to a Gaussian distribution. The parameters of the GCLF were  $\sigma = 1.4$  and  $m^0 = 20$ . This is equivalent to supposing that the GCS is at a distance of 4 Mpc. At this distance, GCs have a stellar appearance, so simulating them with an empirical PSF is adequate. Using an empirical PSF and the DAOPHOT task ADDSTAR, we generated 10 000 artificial GCs uniformly distributed across a  $1000^2$  pixels image. Six different values for the non-convolved variance were used (Fig. 2) and the SBF technique was applied to the final synthetic images in order to recover the total number of GCs. Since all the objects in the image are GCs, it is not necessary to mask the brightest sources, so we used  $m_c = -\infty$  and  $m_1^* = 25$  in equation 7. In this way we obtain  $\sigma_{\text{GC}}^2 = 0.278 N_{\text{TOT}}$ , where  $N_{\text{TOT}}$  is the estimate for total number of GCs in the synthetic image. Finally, the SBF technique will produce for each image the values of  $P_1 = \sigma_{\text{noise}}^2$  and  $P_0 = \sigma_{\text{GC}}^2$ .

In Fig. 3, the power spectrum of the synthetic images for the six different noise levels are presented. Table 5 lists the properties of the synthetic images (columns 1 to 3) and the results of the SBF analysis (columns 4 to 6). The test goes from images with no noise at all (image *a*) to completely noise-dominated images (images *e* and *f*). Here,  $\sigma_{\text{noise}}^2$  is the input noise level,  $N_{\text{GC}}^{\text{in}}$  is the number of GCs introduced in the image,  $P_0$  and  $P_1$  are the SBF results for each image, and  $N_{\text{GC}}^{\text{out}}$  is the total population of GCs estimated using equation 7.

It is very interesting, even in the images with extremely high noise variance, that SBF produces good results. In all cases, there is excellent agreement between the parameters of the input images and those recovered by the SBF technique, both for  $\sigma_{\text{noise}}^2$  and  $\sigma_{\text{GC}}^2$ . We only observe a small systematic excess in the estimated number of GCs. This excess could be due to small differences between the real input GCLF (which includes random effects) and the exact Gaussian-shaped GCLF used to evaluate the final result in equation 7. In order to check this, we calculated  $\sigma_{\text{GC}}^2$  directly from the magnitudes of all the 10 000 GCs added to the images in the following way:

$$\sigma_{\text{GC}}^2 = \sum_{i=1}^{10\,000} f_i^2 = \sum_{i=1}^{10\,000} 10^{-0.8(m_i-25)}. \quad (15)$$

The result was  $\sigma_{\text{GC}}^2 = 2926 (e^-/\text{pixel})^2$ , in full agreement with the obtained SBF results (column 5 in Table 5). With the former test we have shown that SBF is a very powerful, selfconsistent technique, and that very good results can be obtained even with completely noise-dominated images, where traditional techniques do not detect any object.

## 5. Results

### 5.1. Measuring the BGLF and $\sigma_{\text{BG}}^2$

The following treatment is the same for all studied galaxies, but with the aim of illustrating the methodology, we first present the procedure for the galaxy NGC 4874 in detail and then the results for the rest of galaxies.

Once the residual image of NGC 4874 is created, cosmic-ray events and bad pixels are masked. In order to measure  $\sigma_{\text{BG}}^2$ , we must detect all objects brighter than  $4\sigma$  above the zero mean SBF. Using the DAOPHOT task DAOFIND, 649 objects were detected. The photometry was made using ALLSTAR. In Fig. 4, the luminosity function of all detected objects is shown. The solid line represents the BGLF (eq. 11) with  $\gamma = 0.39$  (Tyson 1988) and scaled to our counts. The BGLF in the case of NGC 4874 is:

$$n_{\text{BG}}(m) = 3.17 \times 10^{-13} 10^{0.39m} \left( \frac{\text{galaxies}}{\text{mag} \times \text{pix}} \right). \quad (16)$$

The fit is very good, so we can conclude that almost all point sources are background galaxies, as expected.

Now,  $\sigma_{\text{BG}}^2$  can be estimated using this BGLF and eq. 12. The uncertainty in the background variance must be evaluated taking into account the uncertainty of the BGLF slope as well as possible departures from a pure power-law model. Recent determinations of the *R*-band faint galaxy luminosity function result in slopes in the range  $\gamma = 0.30 - 0.34$  (Steidel & Hamilton 1993). Considering the result by Tyson (1988),  $\gamma = 0.39$ , we have assumed that  $\gamma = 0.30 - 0.40$  is a reasonable range for the slope value. We have done simulations using these two extreme values, resulting in a 20% variation in the background variance. We assume that this 20% is the uncertainty in the background variance. In particular, in the case of NGC 4874, for which  $m_1^* = 24.44$  (see Table 4) and  $m_c = 23.5$ , we obtain:

$$\sigma_{\text{BG}}^2 = (29.4 \pm 5.9) 10^{-4} \left( \frac{e^-}{\text{s} \times \text{pix}} \right)^2. \quad (17)$$

This procedure is repeated for each galaxy. In Fig. 5, the luminosity functions of all detected objects are presented for each galaxy. Again, the solid line represent the BGLF with  $\gamma = 0.39$ , scaled to our counts. Using these BGLFs,  $\sigma_{\text{BG}}^2$  are obtained for each galaxy. Results are listed in Table 6.

## 5.2. Measuring $\sigma_{\text{GC}}^2$ and the GCS properties

As in §5.1, we first describe in detail the procedure used to measure  $\sigma_{\text{GC}}^2$  for NGC 4874 and give the results for the remaining galaxies.

Before computing the power spectrum, all objects brighter than  $m_c = 23.5$  are masked and the ring-shaped regions are created in the galaxy for the analysis of the spatial distribution of GCs. The characteristics of all the regions are given in Table 7 (columns 1 to 3).  $r_{\text{min}}$  and  $r_{\text{max}}$  are the minimum and maximum distances of the selected ring-shaped region to the galaxy center, and  $A$  is the area of this region.

The power spectrum of all the masked regions is then obtained and the SBF evaluated. In Fig. 6, the SBF fit is shown for all the eight ring-shaped regions studied in NGC 4874.

Spatial variations of the PSF along the CCD mosaic may introduce a significant uncertainty in  $P_0$ . To limit this effect, we have used a PSF template for each of the four chips of the WFC. Moreover, in order to evaluate the uncertainty produced along a single chip, SBF fit was repeated for NGC 4874 using eleven PSF templates, which were computed using eleven PSF stars located at different positions of the chip. The differences in  $P_0$  from fit to fit were less than 2%. This 2% was added in quadrature to the sigma of the  $P_0$  measurements of all galaxies. The results for  $P_0$  are listed in column 4 of Table 7.

Subtracting  $\sigma_{BG}^2$  from  $P_0$  in all regions,  $\sigma_{GC}^2$  is obtained. The results for  $\sigma_{GC}^2$  are also given in Table 7 (column 5). Note that NGC 4886 is located in the NGC 4889 ring-shaped region with  $[r_{min}, r_{max}] = [71.9'', 104.7'']$ , so  $\sigma_{GC}^2$  of NGC 4889 in this region has to be also subtracted to the NGC 4886  $P_0$  results.

The GCLF parameters must be introduced in eq. 7 to obtain the number of GCs from  $\sigma_{GC}^2$ . The GCLF for giant ellipticals seems to be universal. There is no empirical evidence showing galaxy-to-galaxy differences in GCLF parameters (Harris et al. 1998). Moreover, Kundu et al. (1999) studied 1057 GCs in the inner region of M87 using *HST* observations. This work shows no evidence for radial variations in the GCLF. Kavelaars et al. (2000) found  $m_V^0 = 27.88 \pm 0.12$  for NGC 4874. This value comes from a constrained fit with  $\sigma = 1.40$ . Assuming a mean value  $(R - I) = 0.55$  and  $(V - I) = 1.01$  for GCs (Ajhar, Blakeslee, & Tonry 1994),  $m_R^0 = 27.42 \pm 0.12$ .

Kavelaars et al. (2000), based on the reviews of Whitmore (1996) and Harris (1999), quote estimates of the intrinsic galaxy-to-galaxy scatters in  $\sigma$  and  $m_R^0$  of 0.05 and 0.15 mag, respectively. Although, from Ferrarese et al. (2000), one might estimate uncertainties twice as large.

In order to include the influence of galaxy-to-galaxy variations in both  $\sigma$  and  $m_R^0$  in our results, we adopted  $\sigma = 1.40 \pm 0.05$  and  $m_R^0 = 27.42 \pm 0.20$  as our fiducial values and tested the influence that 1-sigma variations in both  $\sigma$  and  $m_R^0$  have on  $\sigma_{GC}^2/N_{GC}$ . To this purpose, eq. 7 was used to evaluate  $\sigma_{GC}^2$  using as input parameters the following sets of  $(\sigma, m_R^0)$ : (27.22, 1.40), (27.62, 1.40), (24.42, 1.35) and (27.42, 1.45). The adopted results for  $\sigma_{GC}^2/N_{GC}$  will be the *mean*  $\pm \sigma$  of the sets' results.

For NGC 4874 the next relation is obtained:

$$\sigma_{GC}^2 = (0.067 \pm 0.016) \times N_{GC} \left( \frac{e^-}{s \times \text{pix}} \right)^2. \quad (18)$$

This calibration depends on the photometric calibration of each target field, so it is different for each galaxy. All  $\sigma_{GC}^2/N_{GC}$  calibrations are presented in Table 8, where the ratio

$\sigma_{\text{GC}}^2/N_{\text{GC}}$  is given for the different sets of input parameters (columns 2-5) and for the final adopted value (column 6).

Coming back to NGC 4874, eq. 18 can be used to obtain  $N_{\text{GC}}$  in each region, and multiplying by the area of the selected region, the number  $N_{\text{GC}}^{\text{region}}$  of GCs can be derived (see Table 7, column 7). If we consider the whole galaxy, the total population of GCs is obtained. For NGC 4874, we obtain  $17600 \pm 4100$  GCs. This is the number of GCs in the whole galaxy except the central region, which could not be analyzed due to the difficulty of making a good galaxy profile fit near the center. If the total population of GCs is sought, an estimate of the number of GCs in the central region is required. In this work, we assume that the surface density of GCs in the central region is the same as that obtained in the inner ring-shaped region analyzed in the galaxy. This approximation produces an underestimate of the real number of GCs in the center of the galaxy, but as the size of the region not studied is very small (in some cases negligible), the error introduced is also small. In most galaxies, the estimated number of GCs in the central region is about 5–10% of the total population.

Extrapolating to the central region of the galaxy, we obtain a total population of  $18200 \pm 4100$  GCs for NGC 4874.

In Fig. 7, the radial dependence of the GC surface density is presented. Open dots represent our results obtained with the SBF technique, and filled dots represent the results obtained using the *HST* and traditional techniques (Harris et al. 2000). Interestingly, when analyzed with the SBF technique, ground-based data produce similar results to those of the *HST* except for the galactic halo, where the surface density of GCs obtained in this work is bigger than that obtained by Harris et al. (2000). In particular, the total population obtained by Harris et al. (2000) is  $9200 \pm 1500$  GCs. The result of the present study is closer to that in Blakeslee & Tonry (1995), who obtained a total number of GCs of  $17260 \pm 2030$ .

The total number of GCs can be used to derive the specific frequency,  $S_N$ . The RC3 (de Vaucouleurs et al. 1991) catalogue gives  $V^t = 11.68 \pm 0.11$  for NGC 4874. In order to transform  $V^t$  into  $M_V^{\text{TOT}}$ , some estimation of the Coma cluster distance is required. Kelson et al. (2000) reported the Cepheid distance to Virgo ( $m - M$ ) =  $31.03 \pm 0.16$ . Jensen et al. (2001) measured the SBF distance of the Virgo galaxies NGC 4472 and NGC 4406, obtaining ( $m - M$ ) =  $31.06 \pm 0.10$  and ( $m - M$ ) =  $31.17 \pm 0.14$  respectively. We adopt the mean of the three previous values as our Virgo distance, i. e.  $(m - M)_{\text{Virgo}} = 31.08 \pm 0.14$ . Kavelaars et al. (2000) using the GCLF obtained a relative Coma-Virgo distance modulus of  $4.06 \pm 0.11$ . On the other hand, D’Onofrio et al. (1997), reported a fundamental plane relative Coma-Virgo distance of  $3.55 \pm 0.15$ . Adopting the mean of both,  $3.81 \pm 0.16$ , the Coma distance results  $(m - M)_{\text{Coma}} = 34.89 \pm 0.20$ .

The Coma cluster is located close to the Galactic Pole, with nearly negligible foreground extinction. Using the expressions in Postman & Lauer (1995) for the extinction and the K-correction, and assuming  $E(B - V) = 0.01$  (Baum et al. 1997) and a redshift  $z = 0.024$ , we obtain  $A_R = 0.024$  and  $K_R = 0.025$  mag. After the correction of these effects, we obtain  $M_V^{\text{TOT}} = -23.26 \pm 0.11$  and hence a specific frequency  $S_N = 9.0 \pm 2.8$ .

For the remaining galaxies, SBF analysis results are presented in Table 7, in the same way as for NGC 4874, and for those galaxies that have high enough angular size, the radial structure of those GCSs are shown in Figure 8. The extrapolation to the central regions of all the galaxies is also shown in the first row of each galaxy in Table 7. In Table 9,  $M_V^{\text{TOT}}$  is listed in column 2. For the galaxies IC 3959, MCG +5 –31 –063, NGC 4673, and IC 3651,  $V^t$  does not appear in the RC3 catalogue, and  $M_V^{\text{TOT}}$  was estimated using  $B^t$  and assuming a mean color for these galaxies of  $(B - V) = 1.1$ . In column 3, the distance of the galaxy to the central galaxy NGC 4874 is given, and final results for total populations ( $N_{\text{GC}}^{\text{tot}}$ ) are listed in column 4 and the derived  $S_N$  in column 5.

The distance uncertainty produces an additional error of 18% in the results of  $S_N$ . It must be considered when quoting  $S_N$  for a single galaxy. However, it has the same effect in  $S_N$  for all the Coma galaxies and does not introduce further internal dispersion in any relative distribution of  $S_N$  values of Coma galaxies. In Table 9, the uncertainty in the distance has not been included in the  $S_N$  results.

## 6. Discussion and Conclusions

In the following, we discuss first the scenarios for elliptical-galaxy formation in the light of the obtained results, and second, the possibility that a merging process is at work in Coma.

### 6.1. Elliptical Galaxy Formation Scenarios

We have measured  $S_N$  in 17 elliptical galaxies located in Coma. In Table 9 we present a summary of the obtained results. For each galaxy we show the value of  $M_V^{\text{TOT}}$  (obtained from the RC3 value and adopting a distance modulus for Coma of  $34.89 \pm 0.20$ ), the distance to the central galaxy, NGC 4874, the obtained total population of GCSs, and the result for  $S_N$ . The uncertainty in the distance has not been included in the results, it produces an additional error of 18% in  $S_N$ . These results reveal enormous differences in  $S_N$  among similar galaxies. In particular,  $S_N$  varies by an order of magnitude from galaxy to galaxy. Extreme

cases are: a) at the lower end, NGC 4673 has  $S_N = 1.0 \pm 0.4$ , this value being typical of spiral or irregular galaxies, but surprising for an elliptical galaxy; b) on the other hand, MCG +5 –31 –063 has  $S_N = 13.0 \pm 4.2$  and IC4051 has  $S_N = 12.7 \pm 3.2$ , which are similar to the values found in supergiant cD galaxies, but not in “normal” elliptical galaxies.

Blakeslee et al. (1997) also performed an SBF analysis and reported  $S_N$  results for NGC 4874, NGC 4889 and NGC 4839. They obtained  $S_N = 9.3 \pm 2.0$  for NGC4874;  $5.7 \pm 1.3$  for NGC 4889, and  $4.6 \pm 1.5$  for NGC 4839. These results are compatible (within the error bars) with ours. We obtained for these galaxies  $S_N = 9.0 \pm 2.2$ ,  $S_N = 4.0 \pm 1.2$  and  $S_N = 7.0 \pm 1.9$  respectively. Perhaps there is a small difference in the case of NGC 4839. Note that results reported by Blakeslee et al. (1997) are “*metric* –  $S_N$ ”; i.e.,  $S_N$  calculated within a radius of 40 kpc. If GCs and halo light follow the same radial distribution,  $S_N$  does not change with radius and the “*metric* –  $S_N$ ” would be identical to the global  $S_N$ . The results for NGC 4839 probably indicate that NGC 4839 GCS is more extended than its halo. Indeed, NGC 4839 has the most extended GCS of our sample (see Fig. 8).

Woodworth & Harris (2000) studied *HST* images of IC 4051 and proved that a central location in a rich cluster environment is not required to form a high population of GCs. They obtained a  $S_N$  equal to  $11 \pm 2$ . In our work, IC 4051, a “normal” elliptical near the cluster core, has a high  $S_N$  of  $12.7 \pm 3.2$ . Furthermore, NGC 4874, the central supergiant cD galaxy in Coma, also exhibits a relatively high specific frequency,  $S_N = 9.0 \pm 2.2$ . The remaining galaxies studied have  $S_N$  in the range [2, 7], the mean value being  $S_N = 5.1$ .

Why do IC 4051 and NGC 4673, galaxies with similar absolute magnitudes, have differences of a factor of twelve in  $S_N$ ? Perhaps this is due to differences in the environment. But then, why does MCG +5 –31 –063 have  $S_N$  five times bigger than IC 4041, if both galaxies are located on the border of the Coma cluster core and have the same absolute magnitudes?. In order to study possible relations between  $S_N$  and environment,  $S_N$  versus the distance  $R$  to the central Coma galaxy, NGC 4874 is plotted in Fig. 9. No clear trend is found in this plot, which suggests that  $S_N$  does not depend significantly on the environment in Coma. On the other hand, Fig. 10 shows  $S_N$  versus  $M_V^{\text{TOT}}$  of each galaxy. No relation is found between  $S_N$  and  $M_V^{\text{TOT}}$ . The figure is completely dominated by the dispersion of the points, which is greater than the error bars and must therefore be real.

Formation scenarios for giant ellipticals tend to fall into three basic classes of models: a) in situ models, in which the galaxy condenses by dissipative collapse of gas clouds in one or more major bursts, b) mergers of gas-rich systems, probably disk-type galaxies, and c) accretion of smaller satellites. Various combinations of these extremes are also possible.

In situ models predict a correlation between galaxy properties and the GCS. If we assume

a universal efficiency of GC formation per unit total initial galaxy mass (McLaughlin 1999),

$$\epsilon = \frac{M_{\text{GC}}}{M_* + M_{\text{gas}}} \quad (19)$$

where  $\epsilon$  is the efficiency parameter,  $M_*$  is the mass of the visible stellar component of the galaxy,  $M_{\text{gas}}$  is the mass of gas in or around the galactic halo, and  $M_{\text{GC}}$  is the mass of the GCS, then  $S_N$  must be related with the luminosity of the host galaxy according to:

$$S_N \sim \epsilon \left(1 + \frac{M_{\text{gas}}}{M_*}\right) L_{\text{gal}}^{0.3}. \quad (20)$$

The term  $L_{\text{gal}}^{0.3}$  accounts for the systematic increase in mass-to-light ratio with galaxy luminosity. McLaughlin (1999) predicts the general trend of  $S_N$  with luminosity. The only unknown parameter affecting  $S_N$  would be the ratio of gas to stellar mass. In this paper no evidence is found for a relation between galactic luminosity and  $S_N$ .

On the other hand, if a range of possible GC formation efficiencies is allowed, the merger model can account for the specific frequency range observed for elliptical galaxies (Ashman & Zepf 1992). If the merger model is to explain the *high* –  $S_N$  phenomenon, GC formation must be more efficient in the *high* –  $S_N$  galaxies.

Forte, Martínez, & Muzzio (1982) and Muzzio (1987) have suggested that in clusters of galaxies a population of intergalactic GCs (IGCs) should exist. A galaxy could enlarge its GC population via gravitational capture of IGCs. If they are distributed according to the gravitational potential of the whole galaxy cluster, a relation between  $S_N$  and environment is predicted (White 1987). The current data set shows no indication supporting this prediction.

The fact that no single scenario seems to account for the observed specific frequencies, indicates the history of each galaxy should be deduced individually by suitably combining the models mentioned above (Woodworth & Harris 2000). To this aim, it becomes necessary to extend the observational information on each galaxy. Besides the specific frequency and the radial distribution of the GCS, it is necessary to know the details of the subpopulations (when these exist) and the kinematics of the GCS. In this way, detailed *HST* observations of the extreme cases mentioned above (NGC 4673 and MCG +5 –31 –063) could be a good starting point because these peculiar galaxies can show characteristics found nowhere else, and so offer valuable information in testing the different scenarios.



## 6.2. Subgroups and Merging in Coma

Gurzadyan & Mazure (2001) have recently discovered the existence of three subgroups of galaxies in Coma, one of them associated with the cD galaxy NGC 4874 and the other two with NGC 4889 and NGC 4839. They conclude that the non-stationarity of the dynamical processes at work in the Coma core is due to the merging of small-scale groups of galaxies. In this context, each subgroup formed separately and then the merger between the different groups took place. If this scenario is valid, is there any relation between  $S_N$  and environment and/or  $M_V^{\text{TOT}}$  inside each subgroup?

In order to analyze this question, we restricted our figures to galaxies belonging to Gurzadyan & Mazure (2001) subgroup 2 and studied in this paper: NGC 4874, IC 4012, IC 4041, IC 3976, and IC 3959. In Fig. 11  $S_N$  versus host galaxy magnitude is plotted, while Fig. 12 shows  $S_N$  versus the distance to the galaxy NGC 4874, which is very close to the center of subgroup 2. No relation between  $S_N$  and  $M_V^{\text{TOT}}$  is found from Fig 11. But there is an apparent trend in Fig. 12:  $S_N$  is bigger in high density environments. Is this trend real or is it an artifact of the low number of galaxies considered?. If this result is confirmed, this will be a strong argument in favor of the IGCs model, so the next step in this work will be to enlarge the number of galaxies of the study.

We are very grateful to W. E. Harris for reading a preliminary version of this paper and to J. J. Fuensalida for his helpful comments. This article is based on observations made with the 2.5 m Isaac Newton Telescope operated on the island of La Palma by the ING in the Spanish Observatorio del Roque de Los Muchachos. This research has made use of the NASA/IPAC Extragalactic Database (NED) which is operated by the Jet Propulsion Laboratory, California Institute of Technology, under contract with the National Aeronautics and Space Administration. This research has made use of the Digitized Sky Survey, produced at the Space Telescope Science Institute at Baltimore under U.S. grant NAGW-2166. This research has been supported by the Instituto de Astrofísica de Canarias (grant P3/94), the DGEIC of the Kingdom of Spain (grant PI97-1438-C02-01), and the DGUI of the autonomous government of the Canary Islands (grant PI1999/008).

## REFERENCES

- Ajhar, E. A., Blakeslee, J. P., & Tonry, J. L. 1994, AJ, 108, 2087  
 Ashman, K. M., & Zepf, S. E. 1992, ApJ, 384, 50  
 Baum, W. A. et al. 1997, AJ, 113, 1483

- Bertelli, G., Bressan, A., Chiosi, C., Fagotto, F., & Nasi, E. 1994, *A&AS*, 106, 275
- Blakeslee, J. P. 1997, *ApJ*, 481, L59
- Blakeslee, J. P. 1999, *AJ*, 118, 1506
- Blakeslee, J. P., & Tonry, J. L. 1995, *ApJ*, 442, 579
- Blakeslee, J. P., Tonry, J. L., & Metzger, M. R. 1997, *AJ*, 114, 482
- Bridges, T. J., Carter, D., Harris, W. E., & Pritchett, C. J. 1996, *MNRAS*, 281, 1290
- Chapelon, S., Buat, V., Burgarella, D., & Kissler-Patig, M. 1999, *A&A*, 346, 271
- de Vaucouleurs, G., de Vaucouleurs, A., Corwin, Jr., H. G., Buta, R. J., Paturel, G., & Fouqué, P. 1991, *Third Reference Catalogue of Bright Galaxies* (New York: Springer)
- D’Onofrio, M., Capaccioli, M., Zaggia, S. M., & Caon, N. 1997, *MNRAS*, 289, 847
- Durrell, P. R., Harris, W. E., Geisler, D., & Pruditz, R. E. 1996, *AJ*, 112, 972
- Ferrarese, L., et al. 2000, *ApJ*, 529, 745
- Forte, J. C., Martínez, R. E., & Muzzio, J. C. 1982, *AJ*, 87, 11
- Gurzadyan, V. G., & Mazure, A. 2001, *astro-ph/0102136*
- Harris, W. E. 1987, *ApJ*, 315, L29
- Harris, W. E. 1991, *ARA&A*, 29, 543
- Harris, W. E. 1999, *Lectures for 1998 Saas-Fee Advanced School on Star Clusters*, in press
- Harris, W. E., Harris, G. L. H., & McLaughlin, D. E. 1998, *AJ*, 115, 1801
- Harris, W. E., Kavelaars, J. J., Hanes, D. A., Hesser, J. E., & Pritchett, C. J. 2000, *ApJ*, 533, 137
- Harris, W. E., Pritchett, C. J., & McClure, D. E. 1995, *ApJ*, 441, 120
- Harris, W. E., & van der Berg, S. 1981, *AJ*, 86, 1627
- Jensen, J. B., Tonry, J. L., & Luppino, G. A. 1998, *ApJ*, 505, 111
- Jensen, J. B., Tonry, J. L., & Luppino, G. A. 1999, *ApJ*, 510, 71

- Jensen, J. B., Tonry, J. L., Thompson, R. I., Ajhar, E. A., Lauer, T. R., Rieke, M. J., Postman, M., & Liu, M. C. 2001, *ApJ*, 550, 503
- Kaisler, D., Harris, W. E., Crabtree, D. R., & Richer, H. B. 1996, *AJ*, 111, 2224
- Kavelaars J. J., Harris, W. E., Hanes, D. A., Hesser, J. E., & Pritchett, C. J. 2000, *ApJ*, 533, 125
- Kelson, D. D., et al. 2000, *ApJ*, 529, 768
- Kundu, A., & Whitmore, B. C. 1998, *AJ*, 116, 2841
- Kundu, A., Whitmore, B. C., Sparks, W. B., Maccetto, F. D., Zept, S. E., & Ashman, K. M. 1999, *ApJ*, 513, 733
- Landolt, A. U. 1992, *AJ*, 104, 340
- McLaughlin, D. E. 1999, *AJ*, 117, 2398
- Miller, B. W., Lotz, J. M., Ferguson, H. C., Stiavelli, M., & Whitmore, B. C. 1998, *ApJ*, L133
- Muzzio, J. C. 1987, *PASP*, 99, 245
- Postman, M., & Lauer, T. R. 1995, *ApJ*, 440, 28
- Steidel, C. C., Hamilton, D. 1993, *AJ*, 105, 2017
- Thompson, L. A., & Valdes, F. 1987, *ApJ*, 315, L35
- Tonry, J. L., Dressler, A., Blakeslee, J. P., Ajhar, E. A., Fletcher, A. B., Luppino, G. A., Metzger, M. R., & Moore, C. B. 2001, *ApJ*, 546, 681
- Tonry, J. L., Blakeslee, J. P., Ajhar, E. A., & Dressler, A. 2000, *ApJ*, 530, 625
- Tonry, J. L., & Schneider, D. P. 1988, *AJ*, 96, 807
- Tyson, J. A. 1988, *AJ*, 96, 1
- van der Berg, S., & Harris, W. H. 1982, *AJ*, 87, 494
- West, M. J., Côté, P., Jones, C., Forman, W., & Marzke, R. O. 1995, *ApJ*, 453, L77
- White, R. E. 1987, *MNRAS*, 227, 185

Whitmore, B. C. 1996, in *The Extragalactic Distance Scale*, ed. M. Livio, M. Donahue, & N. Panagia (Baltimore: StScl), 254

Wing, D. L., Harris, G. L. H., Hanes, D. A., & Harris, W. E. 1995, *AJ*, 109, 121

Woodworth, S. C., & Harris, W. E. 2000, *AJ*, 119, 2699

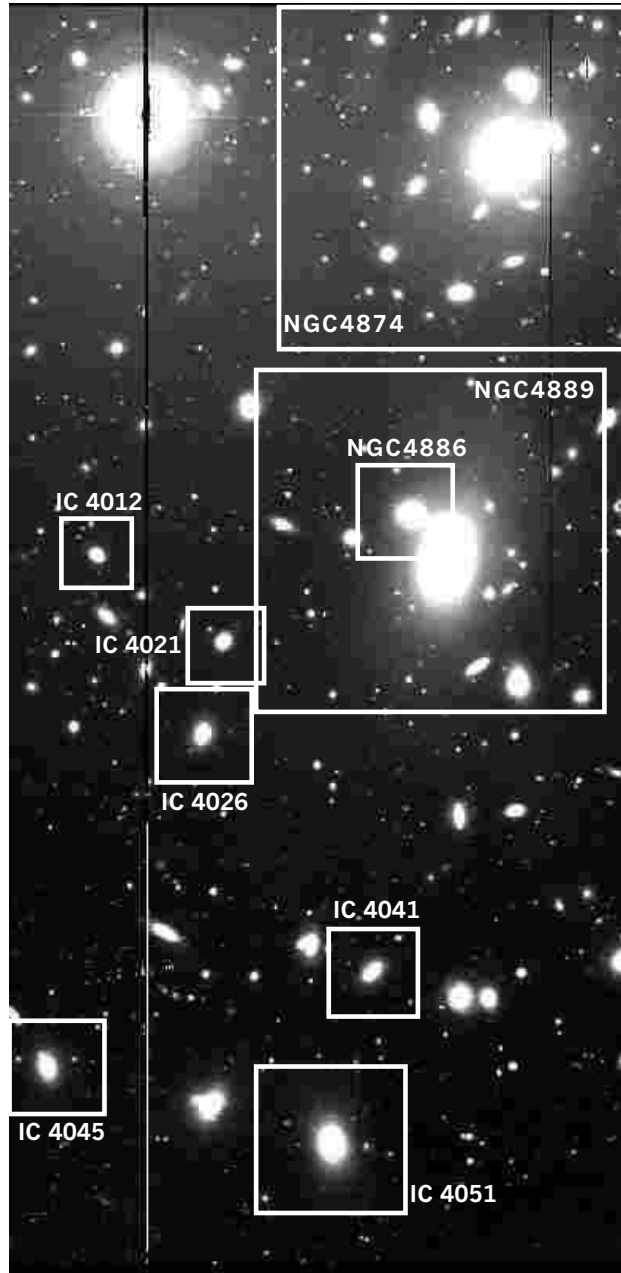


Fig. 1.— Central chip of the CCD mosaic in the target field RC-1. The nine galaxies studied in this chip are labeled.

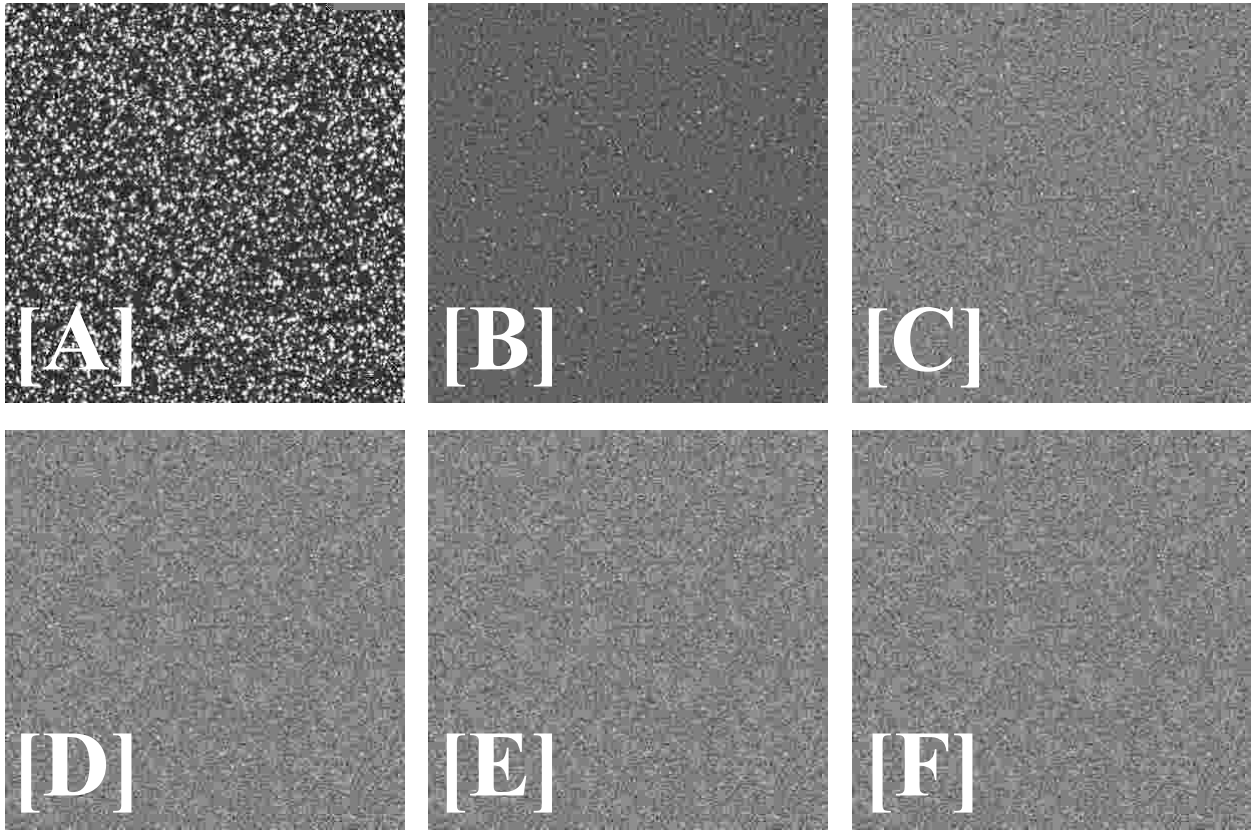


Fig. 2.— Synthetic images generated for the internal consistency test of the SBF to measure GCS properties. Image (a) is noise-free. Noise increases from left to right and from top to bottom. See text and Table 5 for details.

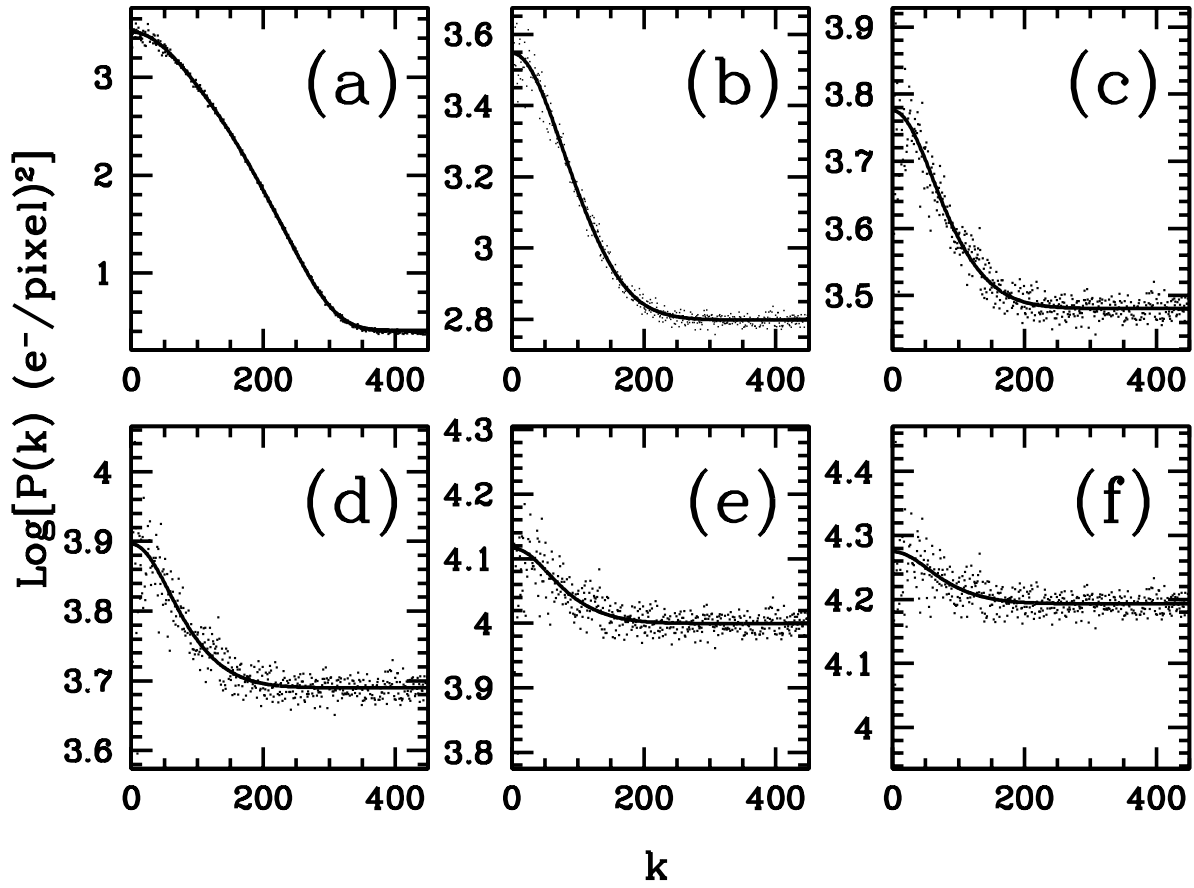


Fig. 3.— SBF analysis of the synthetic images with different noise levels. Points represent the power spectrum of each image, and the solid line is the SBF fitting (eq. 14). See Table 5 for details.

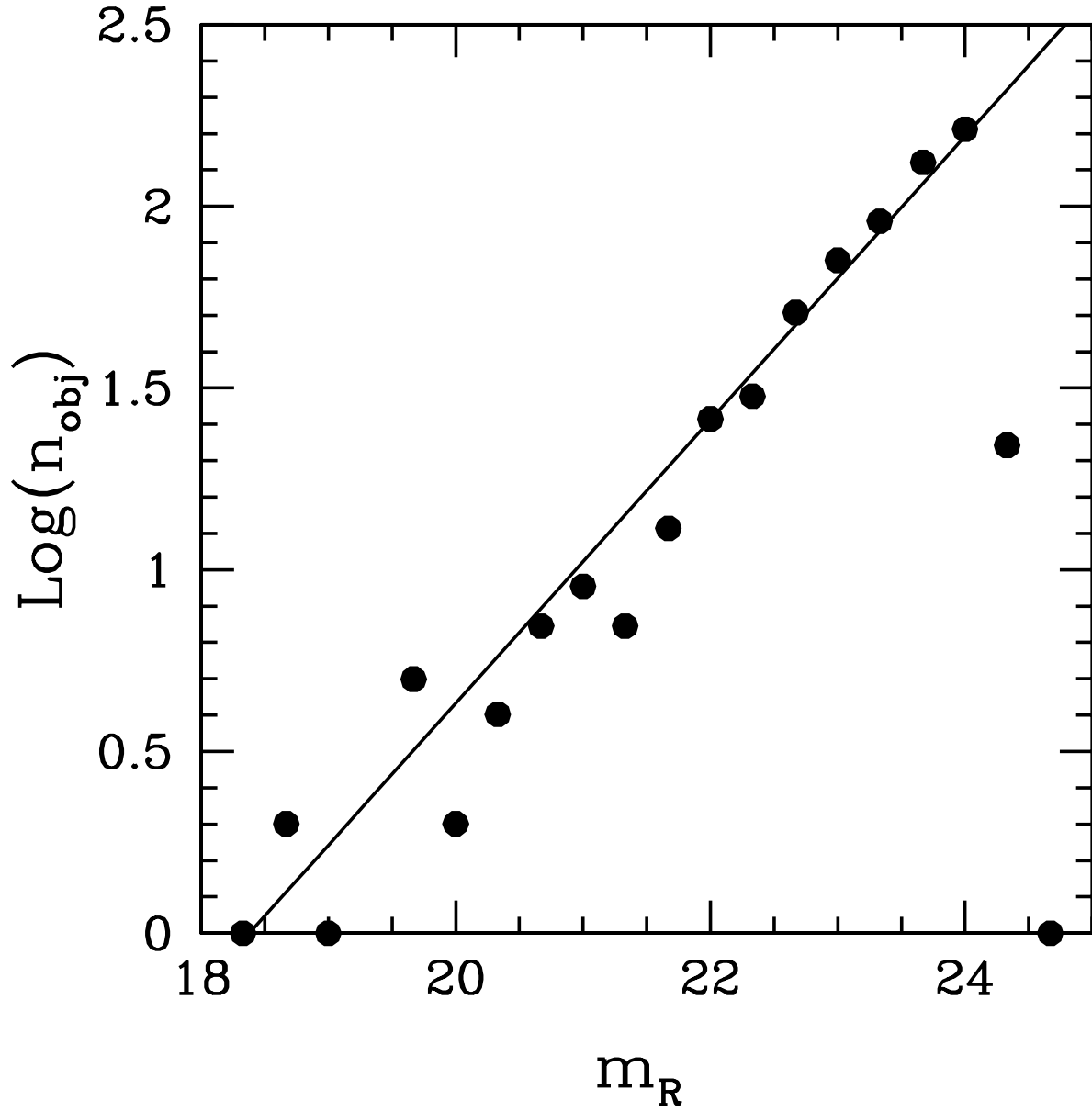


Fig. 4.— Luminosity function of all detected objects in the NGC 4874 image binned to 0.3 mag. Solid line represents the BGLF obtained by Tyson (1988) and scaled to our counts.



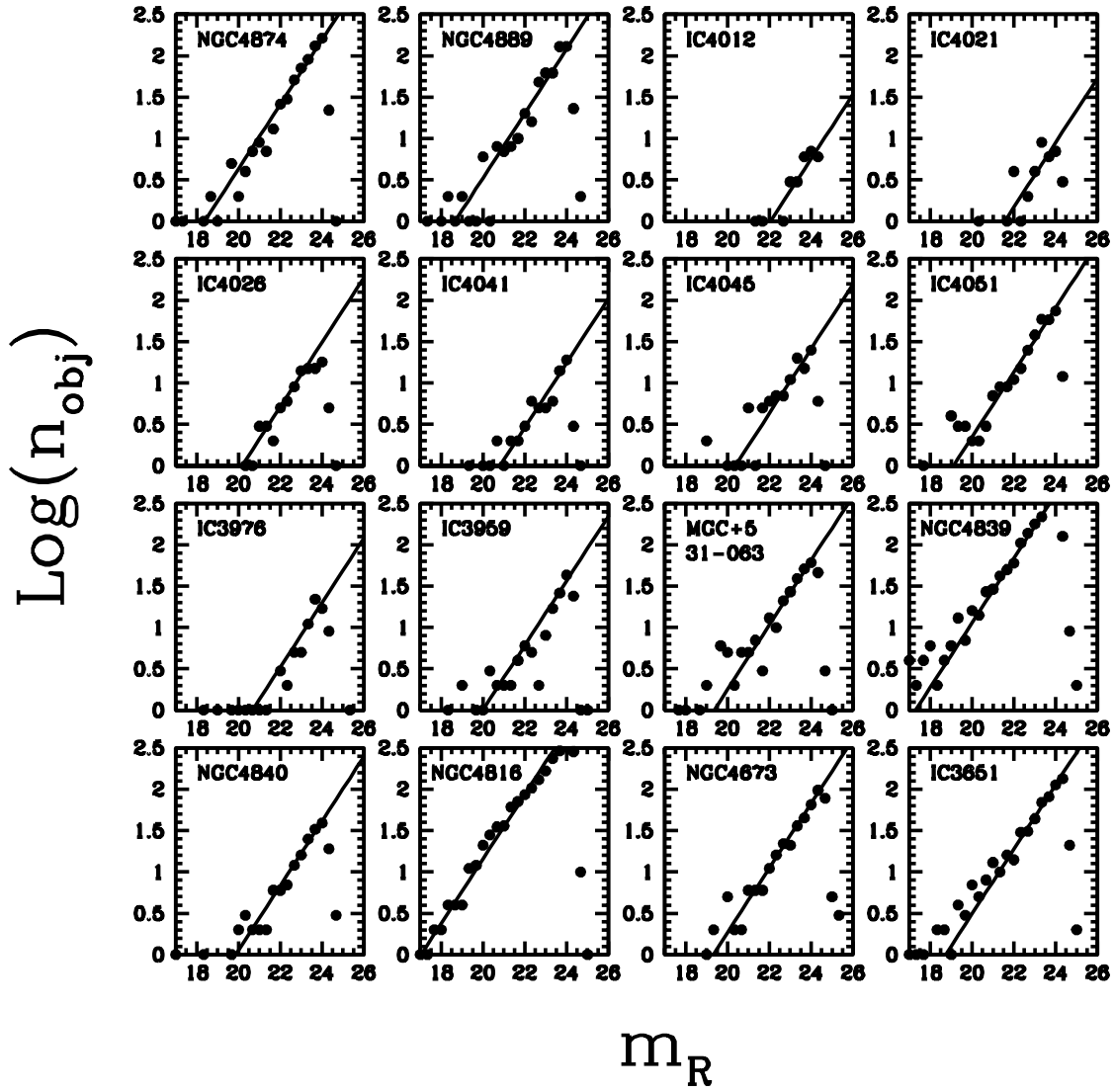


Fig. 5.— Luminosity functions (binned to 0.3 mag) of all detected objects in each galaxy studied. Solid lines represents the BGLF obtained by Tyson (1988) and scaled to our counts.

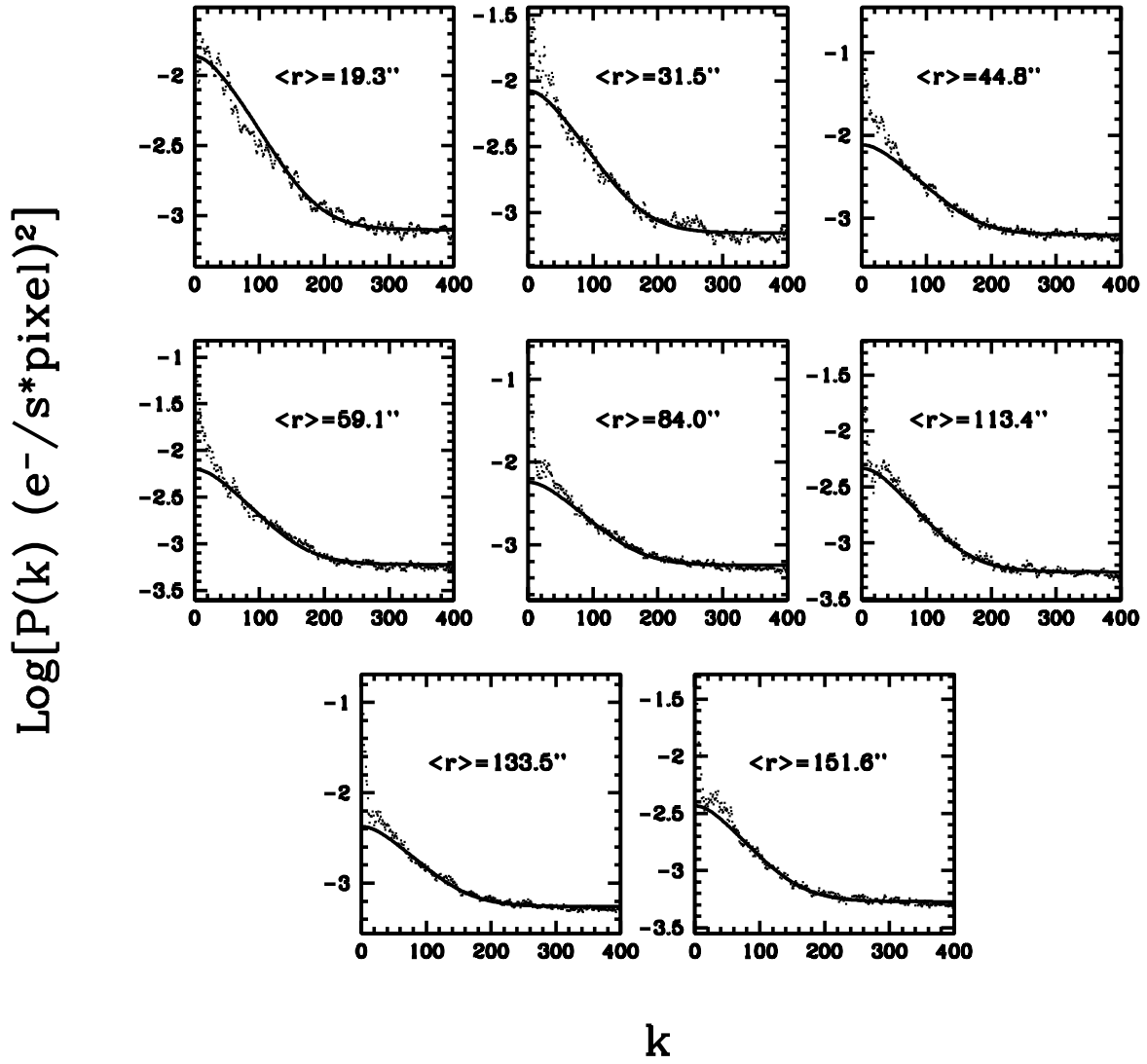


Fig. 6.— SBF analysis of the eight ring-shaped regions studied in NGC 4874. Points are the power spectrum of the masked ring-shaped region, and solid lines are the results of the SBF fit. See details in Table 7.

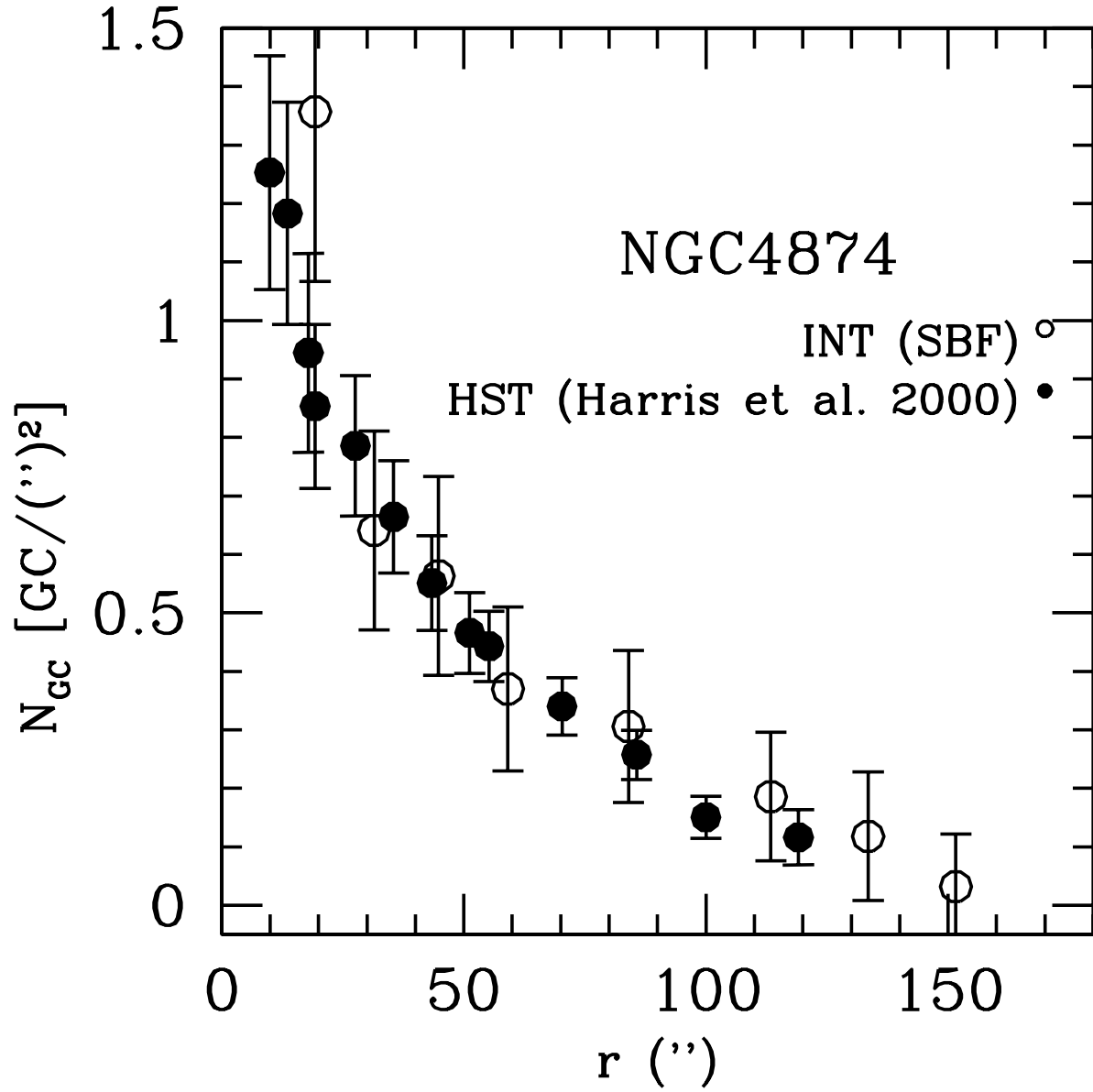


Fig. 7.— Radial dependence of the GCs surface density in NGC 4874. Open dots: results obtained with SBF in this work; Filled dots: results obtained using the HST and traditional techniques (Harris et al. 2000).

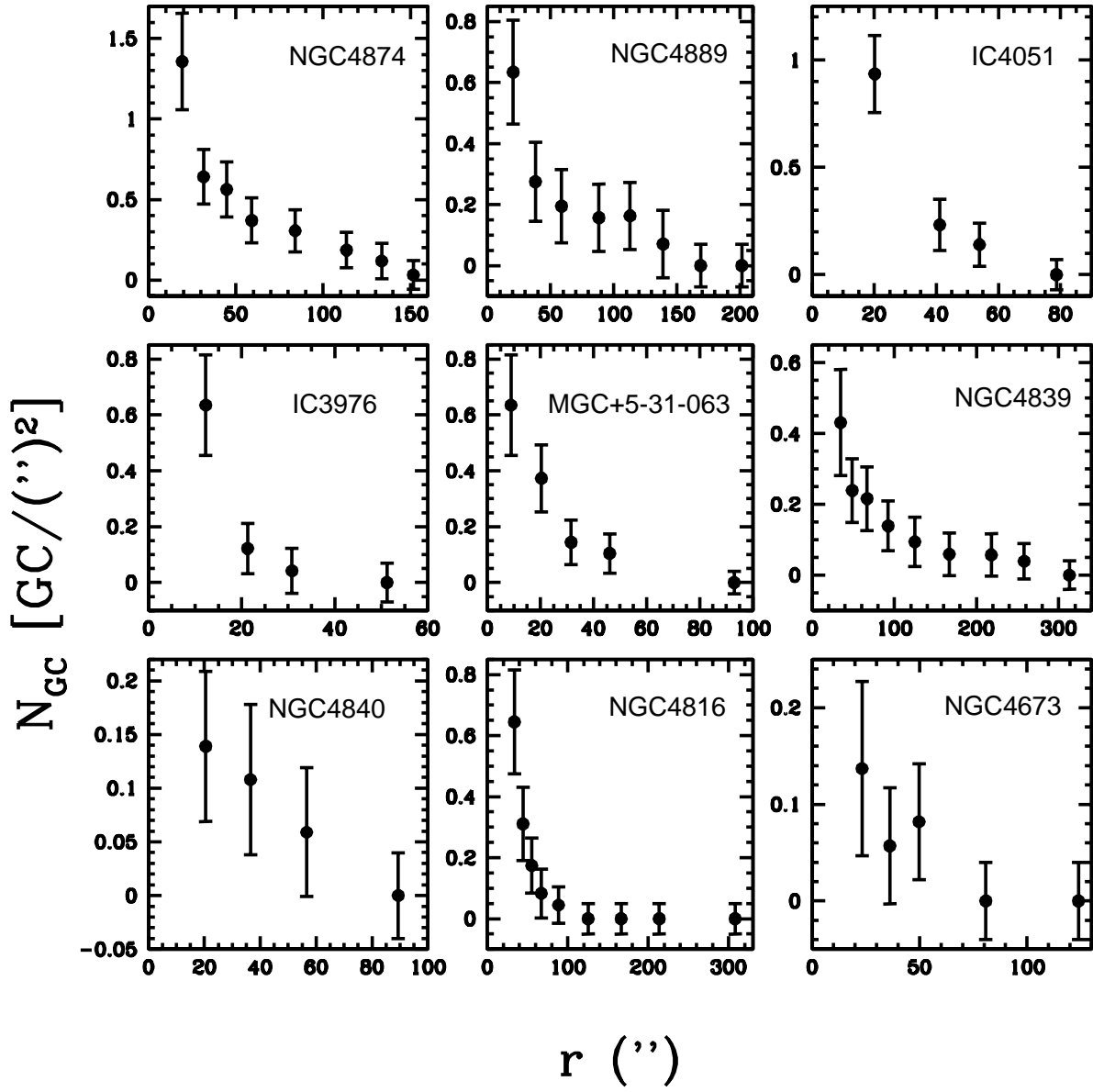


Fig. 8.— Radial structure of the GCS of the nine galaxies with high enough angular size.

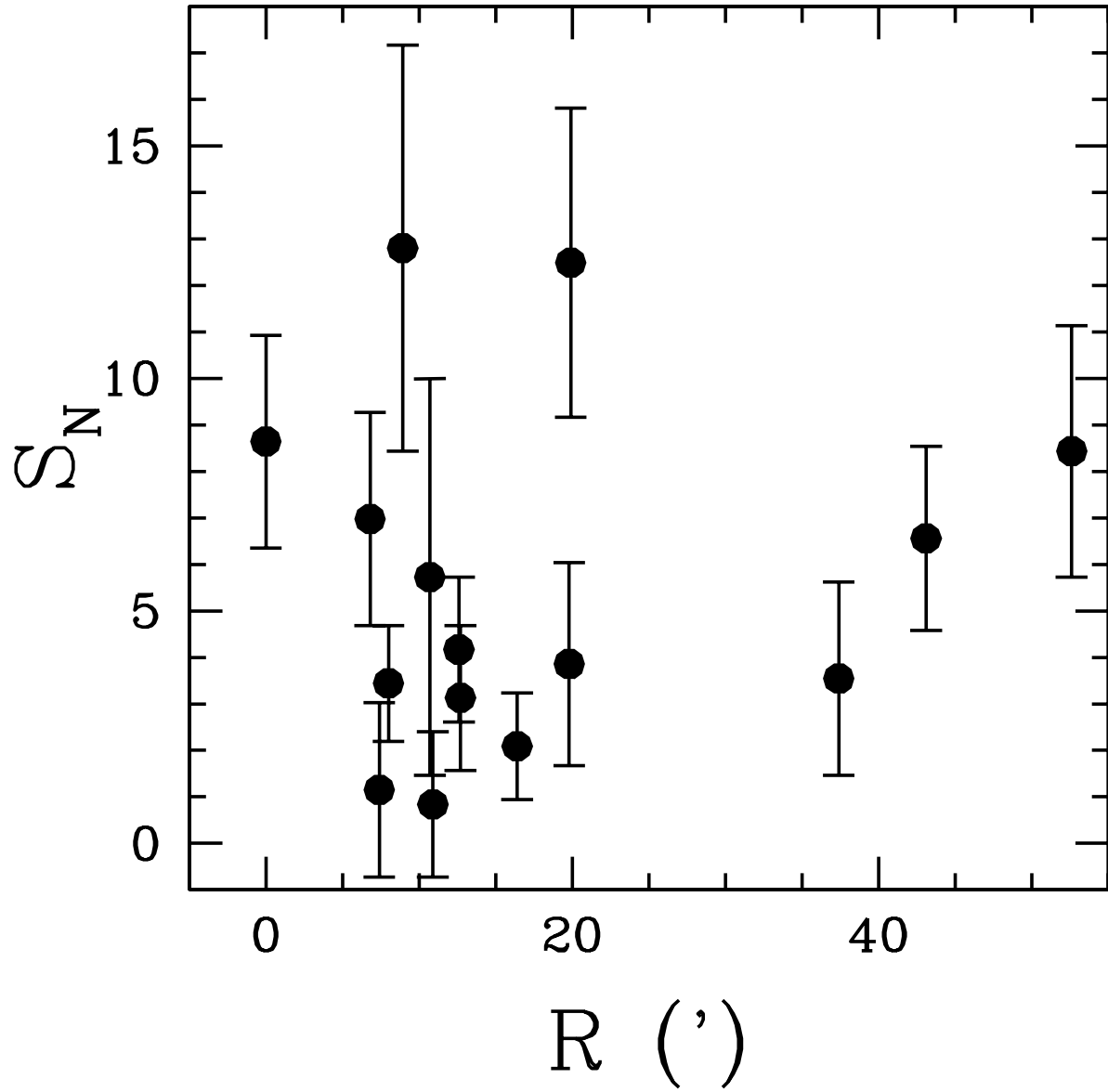


Fig. 9.—  $S_N$  versus the distance of the host galaxy to the Coma cluster center.

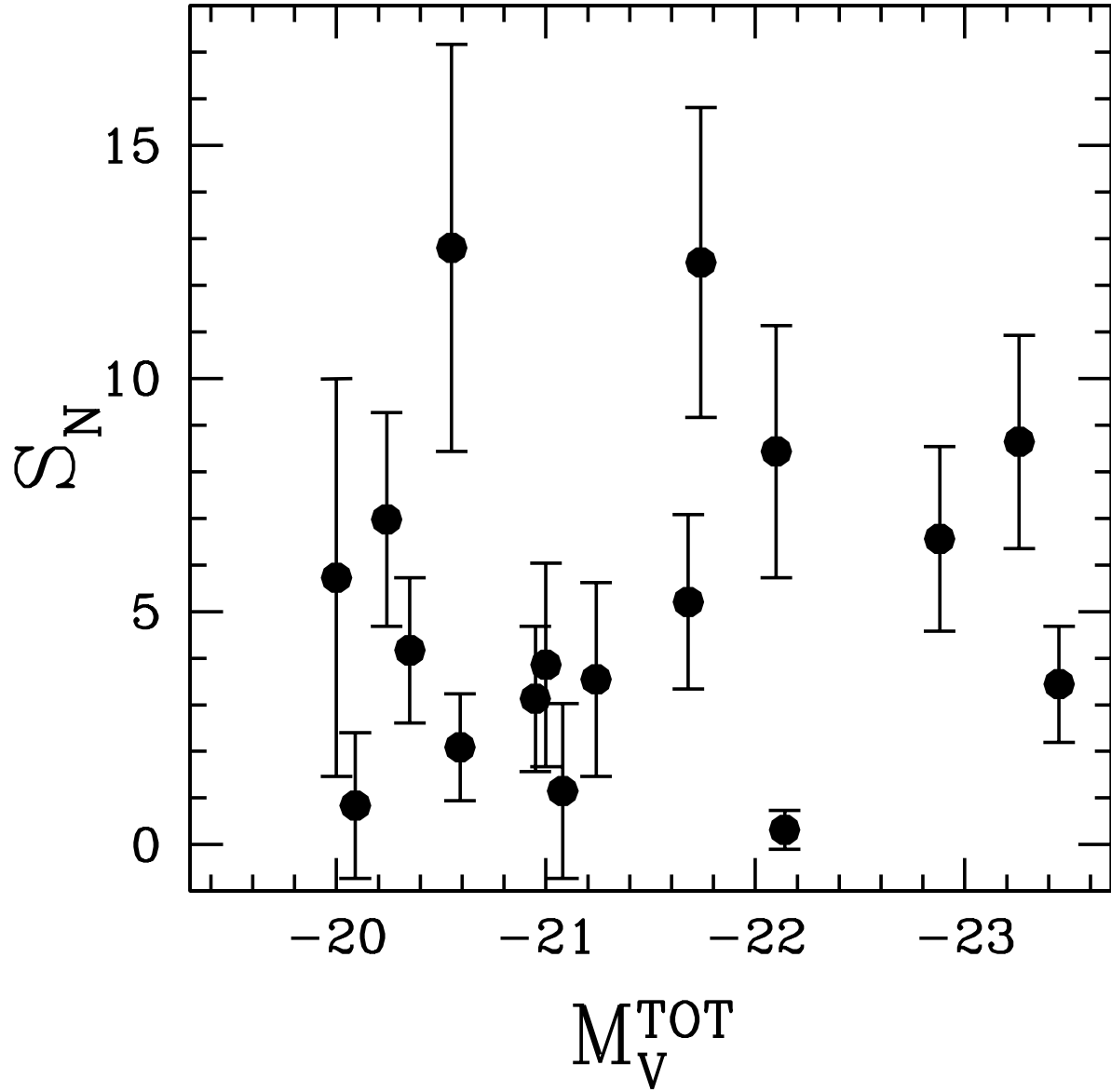


Fig. 10.—  $S_N$  versus  $M_V^{\text{TOT}}$  of the host galaxy.

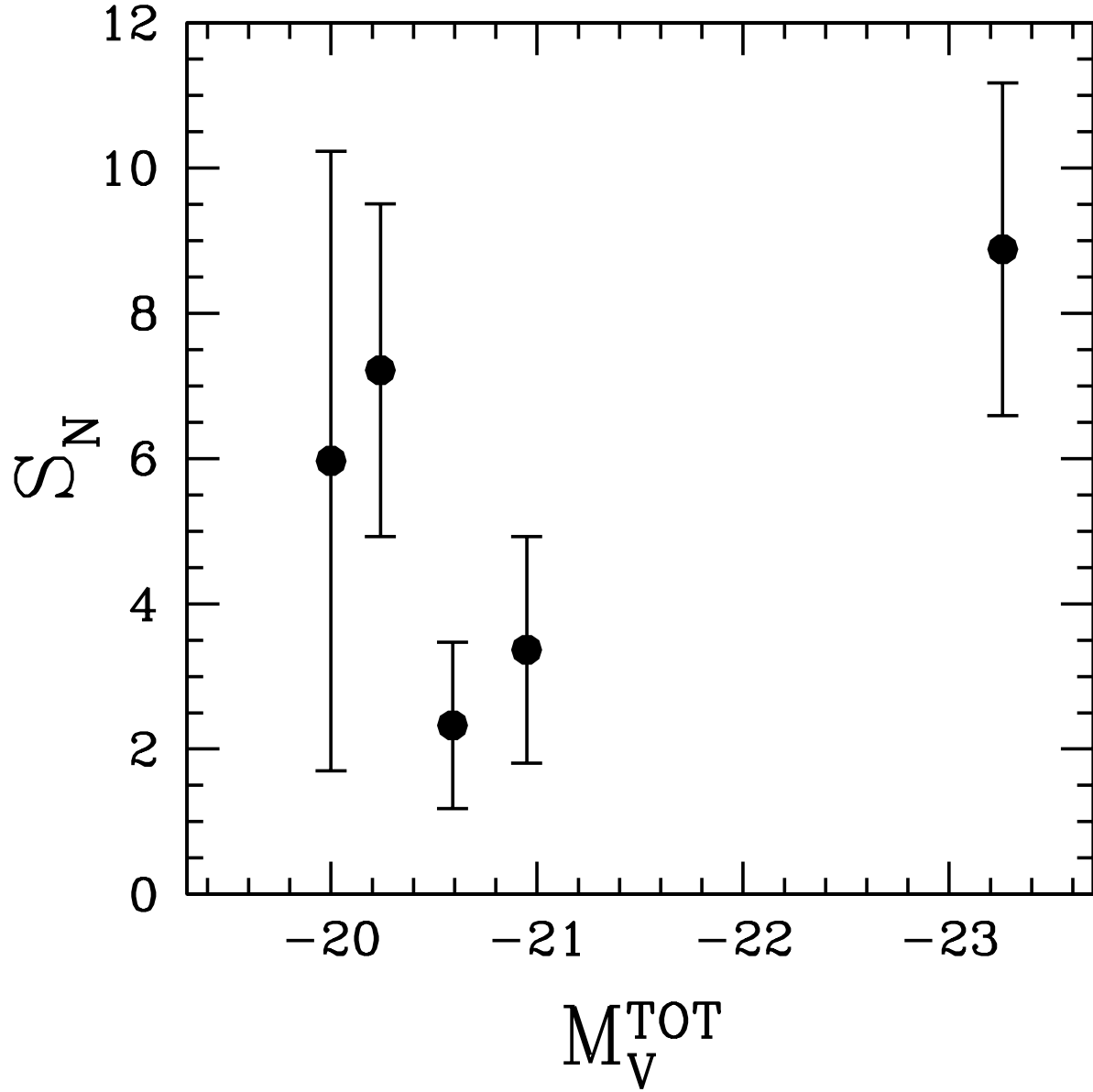


Fig. 11.—  $S_N$  versus  $M_V^{\text{TOT}}$  of the host galaxy (for subgroup 2 of Gurzadyan & Mazure 2001).

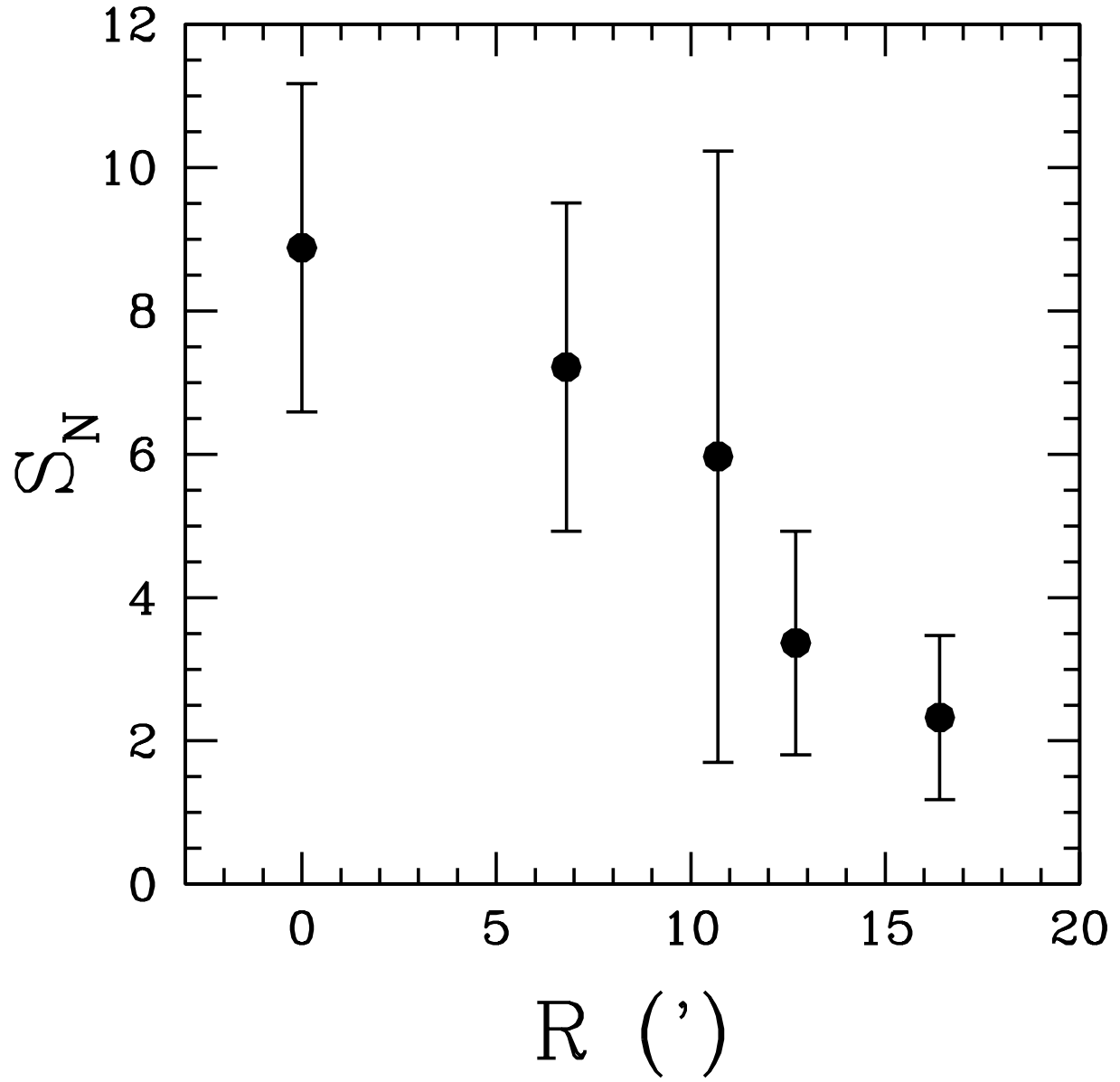


Fig. 12.—  $S_N$  versus the distance of the host galaxy to the Coma cluster center (for subgroup 2 of Gurzadyan & Mazure 2001).



Table 1. Target fields

Target field	$\alpha$ (2000)	$\delta$ (2000)	Galaxies studied
RC-1	13 <sup>h</sup> 00 <sup>m</sup> 14 <sup>s</sup> .4	+28°00′46″.9	NGC 4874, NGC 4889, NGC 4886, IC 4012, IC 4021, IC 4026, IC 4041, IC 4045, I C4051, IC 3976, IC 3959, MCG +5 –31 –063
RC-2	12 <sup>h</sup> 57 <sup>m</sup> 23 <sup>s</sup> .0	+27°43′37″.9	NGC 4839, NGC 4840, NGC 4816
RC-8	13 <sup>h</sup> 45 <sup>m</sup> 26 <sup>s</sup> .0	+27°06′12″.0	NGC 4673
RC-9	12 <sup>h</sup> 40 <sup>m</sup> 53 <sup>s</sup> .1	+26°43′39″.9	IC 3651

Table 2. Summary of observations

Target field	Date	Exposure (s)	Filter	Seeing
RC-1	Apr 25	$6 \times 300$	<i>R</i> (Sloan)	1''1
RC-1	Apr 27	$7 \times 300$	<i>R</i> (Sloan)	1''1
RC-2	Apr 27	$12 \times 300$	<i>R</i> (Sloan)	1''1
RC-8	Apr 27	$12 \times 300$	<i>R</i> (Sloan)	1''0
RC-9	Apr 27	$12 \times 300$	<i>R</i> (Sloan)	1''2

Table 3. Zero points and colour terms of each chip of the CCD

Zero point	Colour term
$a_1=24.422$	$b_1=-0.111$
$a_2=24.671$	$b_2=-0.320$
$a_3=24.682$	$b_3=-0.178$
$a_4=24.654$	$b_4=-0.132$

Table 4. Photometric calibration

Galaxy	$m_1^*$
NGC 4874	$24.44 \pm 0.01$
NGC 4889	$24.44 \pm 0.01$
NGC 4886	$24.44 \pm 0.01$
IC 4012	$24.44 \pm 0.01$
IC 4021	$24.44 \pm 0.01$
IC 4026	$24.44 \pm 0.01$
IC 4041	$24.44 \pm 0.01$
IC 4045	$24.44 \pm 0.01$
IC 4051	$24.44 \pm 0.01$
IC 3976	$24.21 \pm 0.01$
IC 3959	$24.36 \pm 0.02$
MCG +5 -31 -063	$24.36 \pm 0.02$
NGC 4839	$24.22 \pm 0.01$
NGC 4840	$24.22 \pm 0.01$
NGC 4816	$24.37 \pm 0.02$
NGC 4673	$24.43 \pm 0.01$
IC 3651	$24.43 \pm 0.01$

Table 5. Results of the SBF consistency test

Experiment	$\sigma_{\text{noise}}^2 (e^-/\text{pixel})^2$	$N_{\text{GC}}^{\text{in}}$	$P_1 (e^-/\text{pixel})^2$	$P_0 (e^-/\text{pixel})^2$	$N_{\text{GC}}^{\text{out}}$
(a)	0	10000	2.55	$2920 \pm 40$	$10500 \pm 140$
(b)	625	10000	628	$2890 \pm 60$	$10400 \pm 200$
(c)	3025	10000	3027	$2900 \pm 100$	$10400 \pm 400$
(d)	4900	10000	4900	$2900 \pm 150$	$10400 \pm 500$
(e)	10000	10000	9994	$3000 \pm 300$	$10800 \pm 1100$
(f)	15625	10000	15568	$3500 \pm 500$	$12600 \pm 1800$

Table 6. Results for  $\sigma_{\text{BG}}^2$ , in units of  $10^{-4} \times \left(\frac{e^-}{\text{s} \times \text{pix}}\right)^2$ .

Galaxy	$\sigma_{\text{BG}}^2$
NGC 4874	$29.4 \pm 5.9$
NGC 4889	$26.0 \pm 5.2$
NGC 4886	$26.0 \pm 5.2$
IC 4012	$18.0 \pm 3.6$
IC 4021	$16.0 \pm 3.2$
IC 4026	$17.0 \pm 3.4$
IC 4041	$20.0 \pm 4.0$
IC 4045	$20.0 \pm 4.0$
IC 4051	$26.0 \pm 5.2$
IC 3976	$12.1 \pm 2.4$
IC 3959	$15.3 \pm 3.1$
MCG +5 -31 -063	$13.7 \pm 2.7$
NGC 4839	$10.1 \pm 2.0$
NGC 4840	$10.0 \pm 2.0$
NGC 4816	$17.5 \pm 3.5$
NGC 4673	$14.2 \pm 2.8$
IC 3651	$13.7 \pm 2.7$

Table 7. Properties of the ring-shaped regions analyzed in each galaxy and SBF results

$r_{\min}$ (")	$r_{\max}$ (")	$A$ (") <sup>2</sup>	$P_0 \times 10^4$ $\left(\frac{e^-}{s \times \text{pix}}\right)^2$ <sup>(a)</sup>	$\sigma_{\text{GC}}^2 \times 10^4$ $\left(\frac{e^-}{s \times \text{pix}}\right)^2$ <sup>(a)</sup>	$N_{\text{GC}}$ GC/(") <sup>2</sup>	$N_{\text{GC}}^{\text{region}}$
<b>NGC 4874</b>						
0	12.6	452	-	-	-	613 ± 130 <sup>(b)</sup>
12.6	25.9	1410	130 ± 13	101 ± 14	1.36 ± 0.29	1910 ± 410
25.9	37.0	1479	77.0 ± 3.4	47.6 ± 6.8	0.64 ± 0.29	950 ± 250
37.0	52.5	3781	71.2 ± 3.3	41.8 ± 6.8	0.56 ± 0.17	2130 ± 640
52.5	65.6	6408	56.9 ± 3.2	27.5 ± 6.7	0.37 ± 0.17	2370 ± 900
65.6	102.3	13022	52.1 ± 2.2	22.7 ± 6.3	0.31 ± 0.14	4000 ± 1700
102.3	125.1	15031	42.3 ± 1.2	13.8 ± 6.0	0.19 ± 0.13	2800 ± 1600
125.1	141.8	24153	38.2 ± 3.1	8.8 ± 6.7	0.12 ± 0.11	2900 ± 2600
141.8	161.4	18778	31.8 ± 1.2	2.4 ± 6.0	0.03 ± 0.09	600 ± 1700
<b>NGC 4889</b>						
0	10.4	250	-	-	-	158 ± 42 <sup>(b)</sup>
10.4	30.5	3161	73.1 ± 3.3	47.1 ± 6.2	0.63 ± 0.17	2000 ± 540
30.5	45.7	4722	46.4 ± 3.1	20.4 ± 6.1	0.27 ± 0.13	1300 ± 610
45.7	71.9	12767	40.5 ± 3.1	14.5 ± 6.1	0.19 ± 0.12	2500 ± 1500
71.9	104.7	10904	37.7 ± 3.1	11.7 ± 6.1	0.16 ± 0.11	1700 ± 1200
104.7	121.2	6287	38.1 ± 3.1	12.1 ± 6.1	0.16 ± 0.11	1020 ± 690
121.2	157.1	12558	31.3 ± 5.0	5.3 ± 7.2	0.07 ± 0.11	900 ± 1400
157.1	180.3	15044	26.9 ± 3.0	0	0	0
180.3	222.3	22139	26.2 ± 2.1	0	0	0
<b>NGC 4886<sup>(c)</sup></b>						
0	3.5	45	-	-	-	26 ± 9 <sup>(b)</sup>
3.5	24.1	1628	80.2 ± 6.4	42.5 ± 10.2	0.57 ± 0.20	931 ± 325
24.1	33.4	2727	45.0 ± 4.1	7.3 ± 8.9	0.10 ± 0.13	267 ± 354
<b>IC 4012</b>						
0	6.3	127	-	-	-	17 ± 11 <sup>(b)</sup>
6.3	39.0	4605	27.8 ± 3.1	9.8 ± 4.8	0.13 ± 0.09	610 ± 410
39.0	46.7	3692	18.0 ± 1.1	0	0	0
<b>IC 4021</b>						
0	5.0	85	-	-	-	6 ± 6 <sup>(b)</sup>
5.0	27.1	2229	21.0 ± 1.1	5.0 ± 3.4	0.07 ± 0.07	150 ± 160
27.1	46.7	6011	16.4 ± 1.0	0	0	0
<b>IC 4026</b>						
0	6.5	129	-	-	-	78 ± 22 <sup>(b)</sup>
6.5	16.5	694	62.1 ± 6.1	45.1 ± 7.0	0.61 ± 0.17	421 ± 120
16.5	28.2	1915	22.8 ± 3.1	5.8 ± 4.6	0.08 ± 0.08	150 ± 150
28.2	56.7	16810	17.2 ± 1.1	0	0	0
<b>IC 4041</b>						
0	6.4	249	-	-	-	74 ± 30 <sup>(b)</sup>
6.4	25.8	1336	42.2 ± 3.1	22.2 ± 5.1	0.30 ± 0.12	399 ± 160
25.8	44.3	11113	21.2 ± 1.1	0	0	0
<b>IC 4045</b>						
0	13.7	675	-	-	-	146 ± 74 <sup>(b)</sup>
13.7	37.3	3654	36.1 ± 3.1	16.1 ± 5.1	0.22 ± 0.11	790 ± 400
37.3	52.5	3841	23.0 ± 3.0	3.0 ± 5.0	0.04 ± 0.08	150 ± 310
52.5	74.7	13400	19.7 ± 1.1	0	0	0
<b>IC 4051</b>						
0	5.5	126	-	-	-	118 ± 23 <sup>(b)</sup>

Table 7—Continued

$r_{\min}$ ( $''$ )	$r_{\max}$ ( $''$ )	$A$ ( $''$ ) <sup>2</sup>	$P_0 \times 10^4$ $\left(\frac{e^-}{s \times \text{pix}}\right)^2$ (a)	$\sigma_{\text{GC}}^2 \times 10^4$ $\left(\frac{e^-}{s \times \text{pix}}\right)^2$ (a)	$N_{\text{GC}}$ GC/( $''$ ) <sup>2</sup>	$N_{\text{GC}}^{\text{region}}$
5.5	34.9	4093	95.5 ± 4.4	69.5 ± 6.8	0.94 ± 0.18	3830 ± 730
34.9	47.2	4367	43.2 ± 3.1	17.2 ± 6.1	0.23 ± 0.12	1010 ± 520
47.2	60.6	9216	36.4 ± 2.1	10.4 ± 5.6	0.14 ± 0.10	1290 ± 920
60.6	96.9	23739	26.1 ± 2.1	0	0	0
<b>IC 3976</b>						
0	8.0	196	-	-	-	124 ± 35 (b)
8.0	16.7	862	43.8 ± 6.1	31.7 ± 6.6	0.64 ± 0.18	550 ± 150
16.7	25.9	1363	18.2 ± 3.0	6.1 ± 3.8	0.12 ± 0.09	170 ± 120
25.9	36.2	1900	14.2 ± 3.0	2.1 ± 3.8	0.04 ± 0.08	80 ± 150
36.2	66.6	6055	11.5 ± 3.0	0	0	0
<b>IC 3959</b>						
0	11.5	459	-	-	-	105 ± 46 (b)
11.5	33.2	2878	30.2 ± 2.1	14.9 ± 3.7	0.23 ± 0.10	660 ± 280
33.2	44.9	2821	18.1 ± 1.1	2.8 ± 3.3	0.04 ± 0.06	120 ± 170
44.9	89.8	22707	15.2 ± 1.0	0	0	0
<b>MCG +5 -31 -063</b>						
0	1.9	12	-	-	-	8 ± 2 (b)
1.9	15.9	765	55.3 ± 7.1	41.6 ± 7.6	0.64 ± 0.18	486 ± 140
15.9	24.9	1317	38.1 ± 3.1	24.4 ± 4.1	0.37 ± 0.12	491 ± 160
24.9	38.3	2887	23.1 ± 2.0	9.4 ± 3.4	0.14 ± 0.08	420 ± 230
38.3	54.0	7195	20.5 ± 0.7	6.8 ± 2.8	0.10 ± 0.07	750 ± 570
54.0	133.2	43212	13.5 ± 0.6	0	0	0
<b>NGC 4839</b>						
0	31.6	3144	-	-	-	1355 ± 470 (b)
31.6	38.2	1730	32.1 ± 5.0	22.0 ± 5.4	0.43 ± 0.15	750 ± 260
38.2	60.5	3880	22.3 ± 1.1	12.2 ± 2.3	0.24 ± 0.09	930 ± 350
60.5	73.6	6452	22.1 ± 2.1	11.0 ± 2.9	0.22 ± 0.09	1390 ± 580
73.6	111.9	7756	18.2 ± 1.1	7.1 ± 2.3	0.14 ± 0.07	1080 ± 540
111.9	138.5	13850	14.9 ± 1.6	4.8 ± 2.6	0.09 ± 0.07	1300 ± 970
138.5	197.2	13249	13.1 ± 1.0	3.0 ± 2.2	0.06 ± 0.06	780 ± 790
197.2	240.1	24147	13.0 ± 1.0	2.9 ± 2.2	0.06 ± 0.06	1400 ± 1400
240.1	277.4	25663	12.1 ± 1.0	2.0 ± 2.2	0.04 ± 0.05	1000 ± 1300
277.4	349.6	259328	10.3 ± 1.0	0	0	0
<b>NGC 4840</b>						
0	12.9	545	-	-	-	76 ± 38 (b)
12.9	28.1	1705	17.1 ± 1.6	7.1 ± 2.6	0.14 ± 0.07	240 ± 120
28.1	44.9	4182	15.5 ± 1.6	5.5 ± 2.6	0.11 ± 0.07	450 ± 290
44.9	69.2	8811	13.0 ± 0.8	3.0 ± 2.2	0.06 ± 0.06	520 ± 530
69.2	108.9	18358	9.5 ± 0.8	0	0	0
<b>NGC 4816</b>						
0	28.0	2464	-	-	-	1590 ± 420 (b)
28.0	39.5	2357	60.4 ± 6.1	42.9 ± 7.0	0.65 ± 0.17	1520 ± 400
39.5	49.6	3053	38.2 ± 3.1	20.7 ± 4.7	0.31 ± 0.12	950 ± 370
49.6	61.3	4313	29.1 ± 1.1	11.6 ± 3.7	0.17 ± 0.09	750 ± 390
61.3	73.2	6025	23.0 ± 2.1	5.5 ± 4.1	0.08 ± 0.08	500 ± 480
73.2	104.3	18638	20.5 ± 0.7	3.0 ± 3.6	0.04 ± 0.06	800 ± 1100
104.3	145.4	34964	17.2 ± 0.6	0	0	0
145.4	186.1	44838	17.4 ± 1.1	0	0	0



Table 7—Continued

$r_{\min}$ ( $''$ )	$r_{\max}$ ( $''$ )	$A$ ( $''$ ) <sup>2</sup>	$P_0 \times 10^4$ $\left(\frac{e^-}{s \times \text{pix}}\right)^2$ <sup>(a)</sup>	$\sigma_{\text{GC}}^2 \times 10^4$ $\left(\frac{e^-}{s \times \text{pix}}\right)^2$ <sup>(a)</sup>	$N_{\text{GC}}$ GC/( $''$ ) <sup>2</sup>	$N_{\text{GC}}^{\text{region}}$
186.1	241.4	45584	$17.9 \pm 1.1$	0	0	0
241.4	374.0	193496	$16.5 \pm 1.1$	0	0	0
<b>NGC 4673</b>						
0	15.6	770	-	-	-	$105 \pm 69$ <sup>(b)</sup>
15.6	30.8	1810	$24.4 \pm 4.1$	$10.2 \pm 5.0$	$0.14 \pm 0.09$	$250 \pm 160$
30.8	41.3	2370	$18.4 \pm 0.7$	$4.2 \pm 2.9$	$0.06 \pm 0.06$	$135 \pm 140$
41.3	58.1	3140	$20.3 \pm 1.1$	$6.1 \pm 3.0$	$0.08 \pm 0.06$	$260 \pm 190$
58.1	103.5	13364	$14.0 \pm 0.6$	0	0	0
103.5	144.4	36976	$15.5 \pm 0.6$	0	0	0
<b>IC 3651</b>						
0	17.6	1005	$62.9 \pm 6.1$	$49.2 \pm 6.7$	$0.66 \pm 0.17$	$670 \pm 170$
17.6	39.0	3810	$32.2 \pm 2.1$	$18.5 \pm 3.4$	$0.25 \pm 0.10$	$950 \pm 380$
39.0	60.8	6073	$21.0 \pm 0.6$	$7.3 \pm 2.8$	$0.10 \pm 0.04$	$600 \pm 240$
60.8	87.9	12278	$16.7 \pm 0.6$	$3.0 \pm 2.8$	$0.04 \pm 0.05$	$490 \pm 610$

<sup>a</sup>1 pix = 0.333 $''$ .

<sup>b</sup>Estimated number of GCs in the central region of the galaxy. See text for details.

<sup>c</sup>This galaxy is located in the NGC 4889 ring-shaped region with  $[r_{\min}, r_{\max}] = [71.9'', 104.7'']$ , so  $\sigma_{\text{GC}}^2$  of NGC 4889 region has been also subtracted to  $P_0$ .

Table 8.  $\frac{\sigma_{\text{GC}}^2}{N_{\text{GC}}}$  results for different GCLF parameters. See text for details.

Galaxy	(27.22, 1.40)	(27.62, 1.40)	(27.42, 1.35)	(27.42, 1.45)	Adopted
NGC 4874	0.088	0.051	0.060	0.075	$0.067 \pm 0.016$
NGC 4889	0.088	0.051	0.060	0.075	$0.067 \pm 0.016$
NGC 4886	0.088	0.051	0.060	0.075	$0.067 \pm 0.016$
IC 4012	0.088	0.051	0.060	0.075	$0.067 \pm 0.016$
IC 4021	0.088	0.051	0.060	0.075	$0.067 \pm 0.016$
IC 4026	0.088	0.051	0.060	0.075	$0.067 \pm 0.016$
IC 4041	0.088	0.051	0.060	0.075	$0.067 \pm 0.016$
IC 4045	0.088	0.051	0.060	0.075	$0.067 \pm 0.016$
IC 4051	0.088	0.051	0.060	0.075	$0.067 \pm 0.016$
IC 3976	0.058	0.033	0.039	0.049	$0.045 \pm 0.011$
IC 3959	0.076	0.044	0.052	0.065	$0.059 \pm 0.014$
MCG +5 –31 –063	0.076	0.044	0.052	0.065	$0.059 \pm 0.014$
NGC 4839	0.059	0.034	0.040	0.050	$0.046 \pm 0.011$
NGC 4840	0.059	0.034	0.040	0.050	$0.046 \pm 0.011$
NGC 4816	0.078	0.045	0.053	0.066	$0.060 \pm 0.014$
NGC 4673	0.087	0.050	0.059	0.074	$0.067 \pm 0.016$
IC 3651	0.087	0.050	0.059	0.074	$0.067 \pm 0.016$

Table 9. Summary of results

Galaxy	$M_V^{\text{TOT}}$	$R_{\text{NGC4874}}$ (')	$N_{\text{GC}}^{\text{tot}}$	$S_N$
NGC 4874	$-23.26 \pm 0.11$	0	$18200 \pm 4100$	$9.0 \pm 2.2$
NGC 4889	$-23.45 \pm 0.11$	8.05	$9600 \pm 2600$	$4.0 \pm 1.2$
NGC 4886	$-21.08 \pm 0.10$	7.43	$1220 \pm 480$	$1.8 \pm 1.8$
IC 4012	$-20.00 \pm 0.11$	10.68	$620 \pm 410$	$6.2 \pm 4.1$
IC 4021	$-20.09 \pm 0.10$	10.88	$160 \pm 160$	$1.5 \pm 1.5$
IC 4026	$-20.35 \pm 0.15$	12.62	$650 \pm 190$	$4.7 \pm 1.5$
IC 4041	$-20.59 \pm 0.20$	16.38	$470 \pm 160$	$2.7 \pm 1.1$
IC 4045	$-21.00 \pm 0.10$	19.85	$1100 \pm 510$	$4.4 \pm 2.1$
IC 4051	$-21.74 \pm 0.15$	19.95	$6300 \pm 1300$	$12.7 \pm 3.2$
IC 3976	$-20.24 \pm 0.15$	6.78	$920 \pm 250$	$7.4 \pm 2.2$
IC 3959	$-20.95 \pm 0.16^{\text{a}}$	12.67	$880 \pm 330$	$3.7 \pm 1.5$
MGC +5 -31 -063	$-20.55 \pm 0.14^{\text{a}}$	8.93	$2150 \pm 650$	$13.0 \pm 4.2$
NGC 4839	$-22.88 \pm 0.10$	43.12	$10000 \pm 2500$	$7.0 \pm 1.9$
NGC 4840	$-21.24 \pm 0.13$	37.43	$1290 \pm 620$	$4.1 \pm 2.0$
NGC 4816	$-22.10 \pm 0.20$	52.60	$6100 \pm 1400$	$8.8 \pm 2.6$
NGC 4673	$-22.14 \pm 0.18^{\text{a}}$	217.07	$750 \pm 290$	$1.0 \pm 0.4$
IC 3651	$-21.68 \pm 0.14^{\text{a}}$	290.32	$2700 \pm 780$	$5.7 \pm 1.8$

<sup>a</sup>Estimated magnitude. See text for details.